A Techno-economic Perspective on Solar-to-Hydrogen Concepts through 2025

Thomas Grube,[a] Julian Reul,[a] Markus Reuß,[a] Sonya Calnan,[b] Nathalie Monnerie,[c] Rutger Schlatmann,[b] Christian Sattler,[c] Martin Robinius[a] and Detlef Stolten[a,d]

[a] Forschungszentrum Jülich GmbH, IEK-3: Institute of Techno-economic Systems Analysis, D-52425 Jülich, Germany

[b] PVcomB, Helmholtz Zentrum Berlin für Materialen und Energie GmbH, Schwarzschildstraße 3, D-12489 Berlin, Germany

[c] German Aerospace Center, Institute of Solar Research, Solar Chemical Engineering, Linder Hoehe, D-51147 Cologne, Germany

[d] RWTH Aachen University, Chair for Fuel Cells, Faculty of Mechanical Engineering, Kackertstraße 9, D-52072 Aachen, Germany

Abstract

The transition towards a renewable energy-based society is challenged by spatial and temporal imbalances of energy demand and supply. Storage properties and versatility may favor hydrogen to serve as the linking element between renewable energy generation and a variety of sector coupling options. This paper examines four alternative solar-based hydrogen production concepts based on concentrated solar (CSP) or photovoltaic (PV) power generation and solid oxide (SOE) or polymer electrolyte membrane (PEM) electrolysis, namely, CSP-SOE and CSP-PEM, as well as PV-PEM concepts with (PV-PEM I) or without (PV-PEM II) power converters coupling both devices. In this paper, we analyze these concepts in terms of their techno-economic performance in order to determine the levelized cost of hydrogen (LCOH) for the target year 2025, based on different locations with different climate conditions. The analysis was carried out using a broadly applicable computer model based on an hourly resolved time-series of temperature and irradiance. The lowest LCOH was identified in the case of the CSP-SOE and CSP-PEM concepts with 14-17 €-ct/kWh at high-irradiance locations, which clearly exceed the US Department of Energy (DOE) target of 6 $-ct/kWh for the year 2020. Moreover, CSP-SOE also shows the highest hydrogen production volumes and, therefore, solar-to-hydrogen efficiencies. Considering the PV-PEM concepts, we found that the application of power converters for the electrical coupling of PV modules and electrolyzers does not contribute to cost reduction due to the higher related investment costs. A further system optimization is suggested regarding the implementation of short-term energy storage, which might be particularly relevant at locations with higher fluctuations in power supply.

1 Introduction

The extensive implementation of renewable energy technologies is seen by many as the means to achieve a cleaner and more sustainable energy future. Renewable energy (RE) sources such as wind and solar radiation are, by their nature, fluctuating and, therefore, make securing a reliable energy supply more challenging. A possible solution to this is the production of hydrogen that could be cost-effectively stored and subsequently used in a great variety of applications. The sector coupling concept of transferring REs or RE-derived feedstocks to other sectors largely builds on the production of hydrogen for subsequent utilization in the transport, industrial or residential sectors [1, 2, 3]. In addition to wind power-based concepts, electrolytic hydrogen production using solar radiation may offer a promising alternative. However, renewable energy yields are strongly dependent on local solar irradiation levels and diverse technical concepts are presently available at different levels of maturity. The main focus of this study is the analysis of the techno-economic potential of electrolytic hydrogen production via different solar radiation-based pathways for the year 2025. The pathway alternatives considered here range from photovoltaic power generation connected to polymer electrolyte membrane (PEM) electrolysis, to concentrated solar power (CSP) combined with PEM or solid oxide electrolysis (SOE). This study builds on our previous publication by Reuß et al. (2019) [4] that focused on a technical assessment of solar hydrogen production systems comprising PV power generation and PEM electrolysis. The methodical approach to model-based assessment in this study was, initially, to further develop the required subsystem modules based on our previous work: PV and CSP-based power generation, as well as electrolytic hydrogen production via PEM and SOE-based hydrogen production units. These modules were then employed to determine the hydrogen yields at different locations from temperate to subtropical climates. Consequently, the economic performance of the concepts was examined in order to determine the levelized cost of hydrogen (LCOH) at each location.

The relevant literature on the topic of solar-based, electrolytic hydrogen production is divided into three groups of publications. The first considers experimental setups from laboratory-scale devices used as the basis for analyzing larger systems. Clarke et al. [5] coupled an electrolyzer to a solar PV system, proving the general concept of directly coupling PV and EL systems. In that study, a solar-to-hydrogen (STH) efficiency of 4.7% was experimentally achieved [5]. Heremans et al. demonstrated a vapor-fed alkaline anion exchange membrane (AEM) electrolysis system that achieved an STH efficiency of 15% [6]. Meanwhile, Su et al. realized STH efficiencies of up to 6.18% in a directly-coupled PV electrolysis system incorporating a V-shaped concentrator for enhanced sunlight collection [7].

The second group of publications reports on theoretical research that was carried out in order to determine options and potential of solar hydrogen production. Turner et al. presented an overview of hydrogen production alternatives from renewable energy sources [8]. Jacobsson et al. discussed the difference in photoelectrochemical cells and PV-electrolysis systems and proposed a gradual nomenclature for these technologies to structure the research field of solar hydrogen generation [9]. Several other studies review recent research activities and assessment approaches related to the potential of renewable and solar radiation-based

hydrogen production, respectively, on a theoretical scale, without going into details of the physical and chemical modelling of the subsystems [10, 11, 12, 13].

The modelling approaches found in the third group of publications aim to determine the potential of solar hydrogen production, analyzing distinct setups and system combinations, such as PV-PEM systems or photo-electrolysis (PEC) devices. On the one hand, these models can be further divided into bottom-up modelling approaches that were used to model the processes within the subsystems, allowing for the analysis of the dynamics performance of such systems [7, 14, 15, 16, 17, 18, 19]. On the other hand, top-down models that determine hydrogen production with constant efficiencies for the subsystems exist [20, 21, 22, 23, 24]. These models typically consider a broader context and multiple solar hydrogen production pathways, while bottom-up models concentrate on modelling and the optimization of specific setups. Sayedin et al. modelled and optimized a directly coupled PV-PEM system with respect to the subsystem sizes and operating conditions as an example for bottom-up modelling [14, 15]. Garcia-Valverde et al., in turn, followed a similar approach within the optimization of a PV-PEM system with different coupling options [17, 18]. Shaner et al. developed a top-down modeling approach to determine the hydrogen production cost related to two PV-PEM and two PEC systems [22]. Pinaud et al. evaluated the potential of different photo-electrolysis systems for hydrogen production with constant STH efficiencies [21]. Other top-down studies focus on concept exploration and the definition of design guidelines for solar hydrogen-generating devices [20, 23, 24].

Going beyond published research, the specific objective of this study is to more consistently analyze and evaluate the techno-economic potential of candidate solar radiation-based, electrolytic hydrogen production pathways. For this purpose, the study examines the technical concepts that are considered in the literature according to the survey outlined above. The concepts are analyzed and evaluated with respect to their economic performance and level of maturity. This is achieved by describing the fundamental pathway principles and discussing the subsystem's technology readiness levels (TRLs) at first and, secondly, modeling integrated solar hydrogen production systems with consideration to relevant physical and chemical parameters as well, as the systems' operational performance in a bottom-up approach.

After introducing that pathway principles and describing the technology readiness level in the next subsections, Section 2 introduces the relevant details on the concepts and applied methods of analyzing performance and cost. Section 3 presents the results of the analysis and their discussion, followed by the conclusion in Section 4.

1.1 Pathway Principles

Figure 1 displays relevant electrolytic solar-to-hydrogen pathway concepts according to the literature. These concepts are distinguished by power generation and electrolyzer technology and the degree of subsystem integration. The solar-to-hydrogen pathway alternatives analyzed in this study are two PV-PEM and two CSP-EL alternatives, highlighted in blue in Figure 1. With respect to the conclusions drawn in our previous publication [4], PV-PEM III and

PV-PEM IV are only discussed against the backdrop of their general function and technology readiness level.

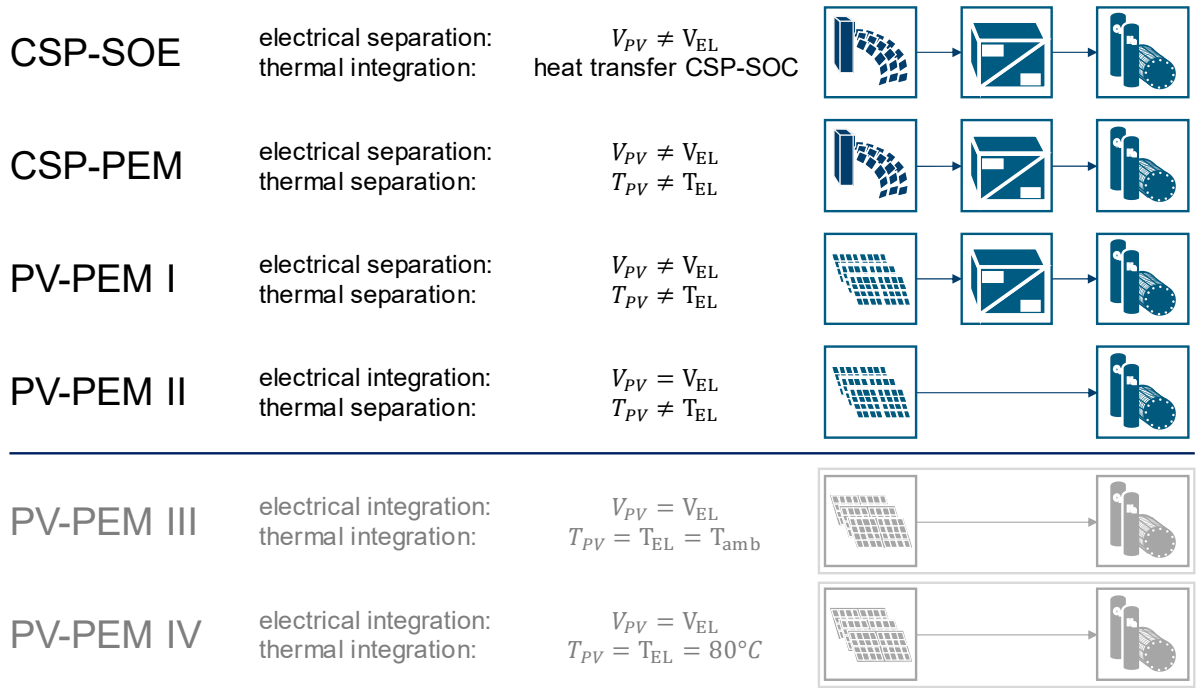

Figure 1. Overview of electrolytic solar-to-hydrogen pathways with different concepts of subsystem integration. CSP: Concentrated solar power generator; EL: Electrolysis; PEM: Polymer electrolyte membrane; PV: Photovoltaic generator; SOE: Solid oxide electrolysis cell.

The **CSP-EL** pathways considered here uses different electrolyzer technologies. While in the CSP-SOE case, the electric power output of the CSP is delivered to a solid oxide electrolyzer, the CSP-PEM concept considers a polymer electrolyte membrane electrolyzer. Utility-scale CSP plants are typically realized as either a solar tower or a parabolic trough. In this work, a solar tower is considered and will be outlined in the following. Figure 2 shows the related system configuration. The electric power generator is comprised of the subsystems' solar tower power block, the power cycle, power electronics and the electrolyzer system. Incoming solar radiation is reflected by the heliostat field to the receiver at the top of the solar tower. The receiver heats a thermal fluid by means of a heat exchanger. Surplus heat is stored in salt-based thermal storage and is used to bridge periods of low irradiation in the daytime or during the night, while sustaining a constant supply of heat to the thermal fluid. A second heat exchanger connects the thermal fluid cycle with the steam cycle for power generation. The CSP plant is then coupled to the electrolyzer via an AC/DC converter. As is mentioned above, the electrolyzer system used in our study is based on either SOE or PEM technology. The SOE system additionally avails the opportunity of heat integration from the CSP plant. The hot product gases from the SOE process are used within the heat recovery system to pre-heat the steam close to the operating temperature of about 800 °C, before it is fed to the electrolyzer.

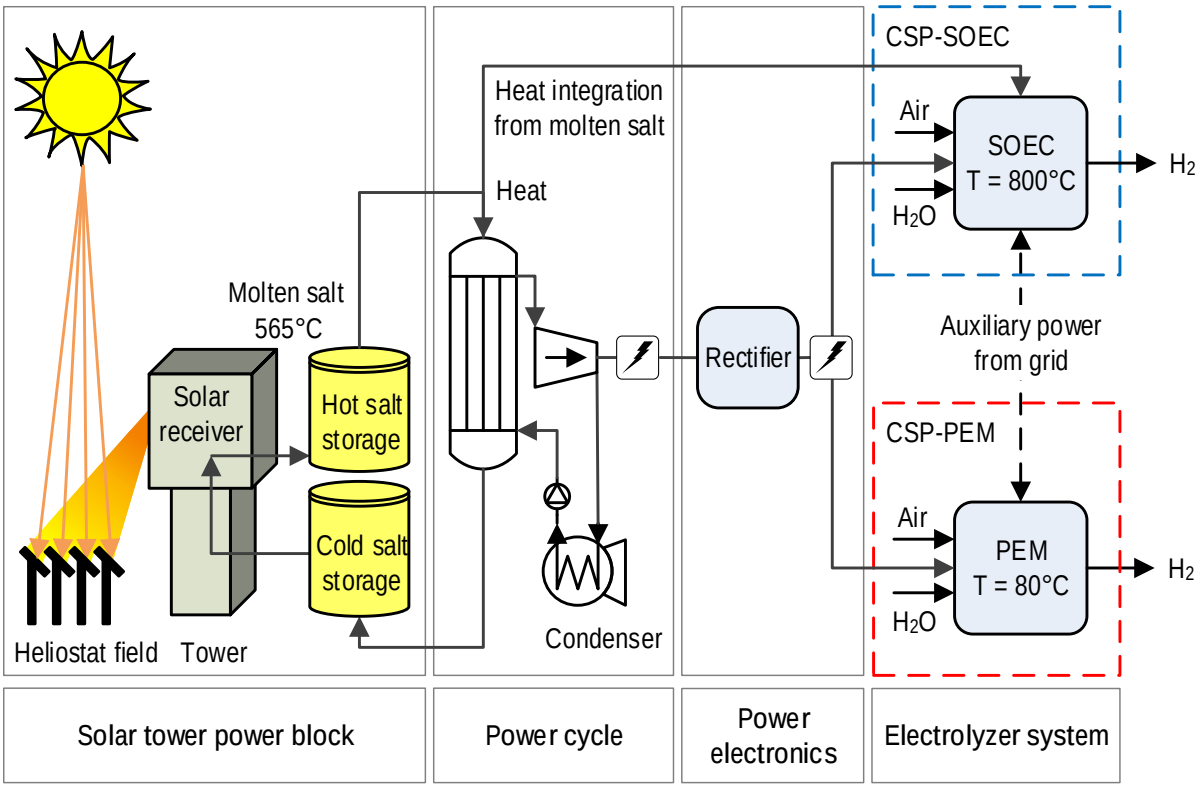

Figure 2. Functional description of CSP-EL pathways. Adapted figure based on Roeb et al. [25].

The **PV-based pathways** analyzed in this study are based on PEM electrolysis and are distinguished by the type of electrical integration, as can be seen in Figure 3. The **PV-PEM I** concept operates with the PV and PEM subsystems being spatially- and thermally-separated and connected with a DC/DC converter. The converter adjusts the electrical output of the PV module to fit the operational characteristics of the electrolyzer. An advantage of the converter is that there are no coupling losses apart from the converter efficiency, which depends on the load level. Furthermore, the individual operating points of the PV and PEM subsystems do not have to be matched during the design phase. For the **PV-PEM II** concept, the PV and PEM subsystems are still spatially- and thermally-separated, but without the power converter.

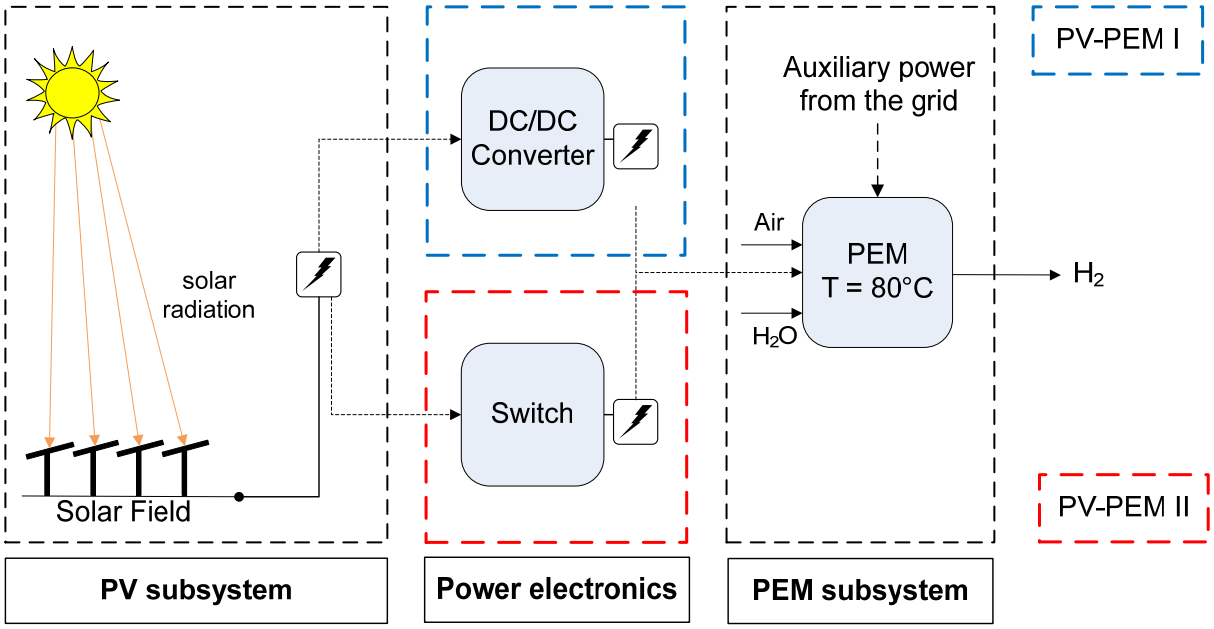

Figure 3. Functional description of the PV-PEM pathways PV-PEM I and PV-PEM II considered in this study. Adapted figure based on Roeb et al. [25].

PV-PEM III and **Photo-electrolysis**, which are not considered in our simulations, show an even further integration level of the PV and PEM components. PV-PEM III omits the use of power electronics, similar to PV-PEM II, and also brings PV and PEM subsystems together spatially. This causes an additional thermal coupling of the subsystems. Photo-electrolysis integrates the principles of photovoltaic power generation and electrolytic hydrogen production into a fully integrated single device. The semiconductor is here directly connected to the catalyst-electrolyte interface, where the hydrogen is generated.

1.2 Technology Readiness Level (TRL)

The solar-to-hydrogen pathways employ diverse technologies with different degrees of maturity, efficiencies and potentials. These divergent criteria are estimated based on information from the literature related to PV, EL and CSP. Based on standard TRL definitions according to Mankins (1995) [26] and EU (2014) [27], these findings are summarized into a TRL estimate for all subsystems under consideration. The relevant information collected in the literature can be found in the supplemental material, section 5.1.

Table 1 summarizes the TRL estimates for the different subsystems. PEM and – despite a lower TRL of 5 – SOE technology are of particular interest in the context of this study, as PEM is expected to be the dominant technology for sector coupling in the future and SOE technology can be beneficially applied in CSP systems due to its high efficiency potential through thermal system integration. These two technologies are therefore considered in this study.

Table 1. TRL estimates of the subsystems based on our literature survey. The underlying information can be found in the supplemental material, section 5.1.

Component Technology	TRL
Photovoltaic (PV) power generation (SHJ)	9
Polymer electrolyte membrane (PEM) electrolysis	8
Solid oxide electrolysis (SOE)	5
Concentrated solar power generation (CSP)	9
Power electronics (PE)	9

SHJ: Silicon heterojunction technology.

The TRLs of the subsystems are linked to derive the TRL estimates related to the individual solar-to-hydrogen concept alternatives considered in this study. On the one hand, none of the described pathways was demonstrated on a commercial or larger laboratory scale. On the other, all of the pathways employ technologies with elevated and high maturity and TRLs of between five and nine. Following this fact, the determination of the TRLs is based on evaluating the prospects of realizing the respective STH pathway on a larger scale with consideration to the availability of the individual subsystems. Table 2 lists the TRL estimates of the different solar-to-hydrogen concepts. In the following, our TRL-related findings and the application potentials of the individual pathways will be briefly discussed.

Table 2. TRL estimates for solar-to-hydrogen pathways.
Concept description – see section 1.1.

Pathway	TRL
PV-PEM I (PV-PEM + power electronics)	8
PV-PEM II (PV-PEM directly coupled)	8
PV-PEM III	7
PV-PEM IV	5
PV-SOE + power electronics	5
(PV-SOE direct)	5
CSP-PEM	8
CSP-SOE	5

The highest TRL is attributed to the concepts of PV-PEM with or without employment of power electronics (PV-PEM I and PV-PEM II) and CSP-PEM, as they incorporate subsystems with the highest individual TRL. Furthermore, the coupling of power generation and electrolysis via power converters does not impose any additional constraints that must be considered. Every subsystem can work independently and has been linked to other technologies in the past [28]. Thus, the theoretical setup could be easily realized, justifying the high TRL of eight for both pathways. The pathway PV-PEM III, directly coupling power generation and hydrogen production, is rated with a lower TRL of seven due to additional operational restrictions. The directly coupled and integrated pathway PV-PEM IV has only been realized on a laboratory scale, with no industrial scale in sight so far [??]. Furthermore, the scaling of such systems would require the development of new technical components and seals. This is different to the pathways discussed above, which incorporate commercially available components coupled in new system layouts. Thus, the directly-coupled and locally-integrated PV-PEM IV pathway is

rated with a TRL of five. All other pathways work with SOE electrolysis, which justifies the TRL rating of five for these.

2 Methods and Assumptions

This section provides more details on the concepts considered in this study and presents the relevant model parameters and constraints, as well as the technical modeling approaches. The individual models of the subsystems are then outlined, before the interaction of the subsystems within the overall system of a solar-to-hydrogen concept is discussed.

2.1 Overall Definitions and Parameters

The calculation of the hydrogen production quantities via the selected pathways was conducted for specific locations based on hourly resolved time series of solar irradiation and ambient temperature. The locations chosen for the calculations were Oldenburg and Freiburg in Germany, Almeria in the south of Spain and Daggett in the Mojave desert of the southwestern United States. Oldenburg and Freiburg are contrasting locations in Germany that resemble locations with a very low (Oldenburg) and elevated (Freiburg) exposure to solar irradiation over the year. Almeria is chosen to represent a Europe-wide and Daggett a world-wide maximum of solar irradiation. For both of the PV-PEM cases, all four locations are considered in this study. The analysis of the two CSP-EL cases is carried out on the basis of data from Almeria and Daggett only. Due to low direct irradiance, CSP plants are not considered to be commercially-feasible in Germany.

With regard to the location-specific analysis, the two input parameters to the simulations are global horizontal irradiation (*GHI*) and ambient temperature. The *GHI* is derived from hourly values of the direct normal irradiation (*DNI*) and the diffuse horizontal irradiation (*DHI*) depending on the tracking process of the solar panels and CSP collectors. The CSP system employs two-axis tracking, which is inherent to this technology, while the PV system is modeled without tracking. The PV modules are oriented southward to the sun, as all observed locations are in the northern hemisphere. The tilt angle of the module's surface is equivalent to the latitude of the location to collect the maximum solar input. We used Typical Meteorological Year data from JRC's Typical Meteorological Data access service [29].

Considering the concept alternatives selected in this study, the subsystems to be analyzed by means of simulation modeling are the photovoltaic module, the concentrated solar power generators, the electrolyzers and the power electronic devices. The technical models are complemented by an economic analysis of the subsystem cost in order to determine the levelized cost of hydrogen for each solar hydrogen production pathway. The cost data is estimated for the reference year 2025 and correlated to the short- to mid-term performance of greenhouse gas reduction technologies.

2.2 Subsystem Models

The subsystems of the hydrogen production pathways considered in this study are the photovoltaic module, electrolysis system and power electronics. Subsystem models related to the PV-based concepts examined in this study are similar to those outlined in Reuß et al. (2019) [4]. The description is therefore short and contains only the most relevant approaches and parameters. For further information, please refer to Reuß et al. [4], where the CSP and SOE subsystems are presented in more detail.

2.2.1 Photovoltaic Module

The PV model used in this study is the same as that in Reuß et al. (2019) [4]. The module data relate to the Panasonic VBHN330SA15 and have been derived from the SAM database [30]. The technical parameters of the module are listed in Table 3.

Table 3. Module parameters. [30]

Parameter	Value	Unit
P_{MPP}, Power at MPP	330.6	W
U_{MPP}, Voltage at MPP	58	V
I_{MPP}, Current at MPP	5.7	A
U_{OC}, Open Circuit Voltage	69.7	V
I_{SC}, Short Circuit Current	6.1	A
U_{oc}, Temperature Coefficient	-0.170	V/°C
I_{sc}, Temperature Coefficient	0.002	A/°C

Also, in accordance with Reuß et al., the *U-I* characteristics are modeled using the equivalent circuit that is displayed in Figure 4.

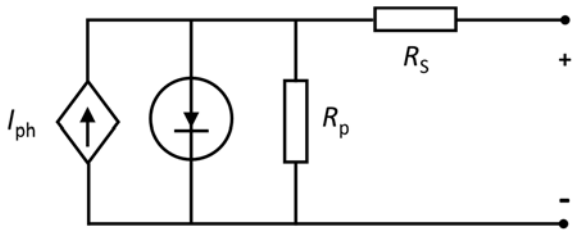

Figure 4. Equivalent circuit of the one-diode-model [31].

The calculation uses a set of equations in accordance with De Soto et al. that require five parameters to outline the equivalent circuit [32] described by equation Eq. 1:

$$I = I_{ph} - I_0 \left[e^{\frac{U+IR_S}{a}} - 1 \right] - \frac{U+IR_S}{R_p} \quad \text{Eq. 1}$$

R_s series resistance
R_p shunt resistance
I_{ph} light current
I_0 diode reverse saturation current
a modified ideality factor

Where parameter ***a*** is defined using Eq. 2:

$$a = \frac{N_s n k T_c}{e} \quad \text{Eq. 2}$$

These five parameters are typically provided by the manufacturer of the PV module in the respective datasheet. The parameters for the PV module of our choice are listed in Table 4, below.

Table 4. Reference input parameters for the one-diode model approach, extracted from the SAM database [30] for the selected Panasonic PV Module VBHN330SJ47.

Parameter		Value	Unit
$R_{S,ref}$	Series resistance	0.741	[Ohm]
$R_{P,ref}$	Ohmic resistance	457.17	[Ohm]
a_{ref}	Ideality Factor	2.3402	[-]
$I_{ph,ref}$	Photo current	6.08	[A]
$I_{0,ref}$	Saturation current	6.88×10^{-13}	[A]
T_{NOCT}	Normal Operating Cell Temperature	43.8	[°C]

2.2.2 CSP System

The concentrated solar power technology considered in this study is a molten salt solar tower, which is a point-focusing system that can heat salt to temperatures above 500 °C. This technology uses molten salt as both the heat transfer fluid and the thermal storage medium. If the storage is designed appropriately, it can allow for continuous operation and such technology is also currently commercially-available [33]. For this study, a thermal storage capacity of 16 full load hours was considered.

The parameters have been derived from the Greenius database [34] and the simulation was performed with the Greenius software, which was developed in order to provide performance calculation algorithms with hourly resolutions for concentrating solar power plants. The calculations are based on technology-specific parameters and the relevant location-specific meteorological data such as solar irradiation values and ambient conditions, as well as the wind direction and speed.

The most important power plant components and the associated parameters are subdivided in Greenius as follows:

(i) Collector and collector field (including geometric data, collector-specific values, field geometry, selection of heat transfer fluid)
(ii) Thermal storage (including the type of storage and storage capacity)

(iii) Power block (rated power)

The parameters of the overall CSP system are listed in Table 5.

Table 5. Parameters for the CSP technology design.

Site Position and Orientation	Almeria (Spain)	Daggett (USA)	Dimension
Latitude	36,83	34,85	°N
Longitude	-2,45	-116,8	°E
DNI	1918	2723	kWh/m²
CSP technology			
Solar tower			
Heat transfer fluid	Molten salt		
Heliostat field			
Heliostat reflective area	121:3	121.3	m²
Clean mirror reflectivity	0.94	0.94	
Total reflective area	1,118,626	910,440	m²
Tower Height	182.5	176.3	m
Receiver			
Receiver Intercept Power	500	500	MW
Receiver Inlet Temperature	292	292	°C
Receiver Outlet Temperature	565	565	°C
Receiver Outlet Power	433	440	MW
Efficiency of heat transfer fluid pump	98	98	%
Powerblock and storage			
Nominal electrical output	70.4	70.4	MW_{el}
Type of storage	Two-tank molten salt		
Thermal storage capacity	2600	2600	MWh

2.2.3 Rectifier and Power Converter

Two types of power electronic devices were used for the modeling in this study, namely a rectifier and a DC/DC converter. The power converter was used to adjust the DC power output of the PV module to fit the DC power characteristics of the electrolyzer within the PV-PEM I concept. The rectifier transforms the alternating current from the CSP plant into direct current, which is then used as the input for the electrolysis. The efficiencies of both components are dependent on the actual load state and the correlations were derived from the SAM database [35]. We assume that the power electronics are not capable of operating above the design point for longer time periods. For this reason, the input power into the power electronics must be kept below or at the nominal power level across the entire operational range. This is achieved by curtailing the input power to the nominal power in the case of an energy excess of above 5%.

2.2.4 PEM and SOE Electrolyzer

The modeling approach of the two electrolyzer types, SOE and PEM, are based upon the characteristic polarization curve, which depicts the dependency between the current density *j* and voltage *U*.

The operational behavior of the SOE is approximated with a linear equation, as the activation overpotentials decrease due to improved reaction kinetics at the operating temperature of 700-800 °C. The following reference points are used [36, 37, 38, 39]:

$$j_0 = 0\,\frac{A}{cm^2};\; U_0 = 0.95\,V \qquad \text{Eq. 3}$$

$$j_1 = 0.75\,\frac{A}{cm^2};\; U_1 = 1.1\,V \qquad \text{Eq. 4}$$

The cell efficiency of the SOE is assumed to be constant across the entire operational range. This is due to two opposing effects, which are both proportional to the load of the electrolysis system. On one side, the cell efficiency increases with decreasing partial load. On the other side, the heat demand increases proportionally with decreasing partial load, as the electrolyzer is not operated under thermo-neutral conditions. The constant cell efficiency at the thermo-neutral point of 113% exceeds 100% because the actual cell voltage is below the water-splitting potential of 1.23 V. Similar to the PEM case, the electrolyzer stack current I_{SOE} is calculated by multiplying the current density j by the active electrode area A_{SOE}. This area is determined within the design phase of each pathway and is optimized depending on the location-specific solar irradiation and power characteristics of the employed PV subsystem. The active electrode area also defines the installed capacity of the electrolysis system. The optimization considers the most cost-efficient relationship of the installed electrolysis to PV capacity.

For the PEM electrolyzer, the model for determining the *U-j*-curve is, as in Reuß et al. (2019) [4], based on Tjarks (2017), Tjarks et al. (2018) and Stolten et al. (2016) [40, 41, 42]. The respective equations are:

$$U_{cell} = 1.185\,V - \alpha(T) \times \ln\left(\frac{j}{j_0(T)}\right) + j \times (R_{ion}(T) + 0.025\Omega + 0.096\Omega) \qquad \text{Eq. 5}$$

$$\eta_{EL,cell} = \frac{H_u}{2*e*N_A*U_{cell}} \qquad \text{Eq. 6}$$

The PEM electrolyzer current I_{PEM} is the product of the current density j and the electrochemically-active area A_{PEM}.

In addition to the losses within the electrolysis cell, the auxiliary power of the balance-of-plant (BoP) components such as pumps and heaters must be considered. Within this model, the auxiliary power of the SOE and PEM electrolysis is assumed to be a fixed share of the electrolyzer systems' nominal power $P_{EL,nom}$ across the entire operational range. For the SOE and PEM electrolysis, this share is set to 2% and 5%, respectively. Furthermore, the auxiliary power demand has no influence on the system efficiency of the electrolysis system, as it is assumed to be covered by the connected power grid. The power that is drawn from the grid is also accounted for within the economic analysis. Faradaic losses are neglected in this analysis, as the electrolysis system is operated under atmospheric conditions. The operational limit is addressed by curtailment in the case of excess voltage above the nominal system voltage in order to avoid increased cell decay. The pathways, which incorporate power electronics, decrease the power supply to the electrolyzer to the maximum voltage input. For the PV-PEM II

systems that do not contain a converter between the PV and EL subsystems, the power supply is cut to zero, when the input voltage exceeds the nominal voltage input by 5% or more.

2.3 Subsystem Interaction and Coupling

Depending on which hydrogen production pathway is considered, the interaction and coupling of the subsystems differ (cf. Section 1.1). This study considers four different STH pathways, each with an approximate solar collection area of ca. 1 km². The functional schemes of these pathways are displayed in Figure 1.

Hydrogen production via a CSP plant connected to an electrolyzer is determined by considering two alternative electrolysis technologies. The pathway CSP-SOE uses the SOE-technology to generate hydrogen from electricity and heat. As the SOE electrolyzer operates at high temperatures of 700-800 °C, the possibility of heat integration from other processes exists. This model considers heat integration from the molten salt cycle of the CSP plant (see Figure 2). The integrated heat is deployed for pre-heating and steam generation before the feed steam is introduced into the electrolyzer. The nominal size of the CSP plant is set to 70 MW_e, while the electrolyzer's capacity is equivalent to the CSP system's nominal power. In order to achieve this, the aperture area of the CSP plant in Almeria is set to ca. 1.12 km² and in Daggett to 0.91 km². The divergence is attributed to different solar irradiation levels between the locations. The pathway CSP-PEM couples the CSP-plant to a PEM electrolysis stack in which a rectifier is employed to convert the alternating current of the CSP plant into direct current. The efficiency of the rectifier is also dependent on the partial load, as depicted below, in section 3.2.

The nominal power of the electrolysis system for the pathways PV-PEM I and PV-PEM II is subject to optimization because there is a trade-off to be made between investment costs and electrolysis efficiency. Related to this optimization, the ratio of electrolysis and PV power is varied within an interval of 0.5-1 of the nominal power for each location. The ratio that leads to minimal hydrogen production cost is used as the design point. For the PV-PEM I concept, it is assumed that the nominal power of the power electronics is equal to that of the electrolysis system. The result of the optimization method is shown in Section 3.2. The operating point for PV-PEM II is found by overlaying the *U-I*-curves of the subsystems. An electrolysis cell operates between 1.5-2 V, while the PV module has an output voltage of about 45 V. In order to approximate the operating points, the voltage of the electrolyzer is multiplied by the number of electrolysis cells, so that an optimal fit of operating points is accomplished. This adjustment is performed during the design phase. Whenever the operational conditions deviate from the nominal design point, the EL curve does not cross the PV curve close to the Maximum Power Point (MPP) of the PV Module. This results in losses, as there is only part of the maximum PV power output being harnessed. These coupling losses then lead to the definition of coupling efficiency [43]:

$$\eta_c = \frac{P_{OP}}{P_{MPP}} = \frac{J_{OP} * U_{OP}}{J_{MPP} * U_{MPP}}$$ Eq. 7

The nominal power of the PV subsystem is related to the solar collection area of the CSP plant to approximate the solar input energy of both pathways. The aperture area is set to 1 km², which leads to a nominal power of 197.6 MW_e for the PV subsystem.

2.4 Economic Analysis

This section outlines the necessary investments and operational costs (*OPEX*) of the PV, CSP and EL subsystems. These parameters are used to find the overall cost for all of the pathways under consideration. The economic analysis is conducted for the reference year 2025.

Investment in the hydrogen production pathways is calculated as the product of specific investment [€/kW_p] and the installed nominal power [kW_p], while the operational cost *OPEX* [€/a] is determined from the operation and maintenance (O&M) cost, which are estimated using a given percentage of the investment cost:

$$INVEST = \text{Specific Investment Cost} * \text{Installed Nominal Power}$$ Eq. 8

$$OPEX = O\&M \times INVEST$$ Eq. 9

Section 3.1 presents the total annual cost (*TAC*) [€/a] as the sum of the annuity factor multiplied by the investment and operational costs (*OPEX*):

$$TAC = ANN \times INVEST + OPEX$$ Eq. 10

The annuity factor *ANN* is determined with a fixed interest rate *i* of 8% and the depreciation period *n*:

$$ANN = \frac{(1+i)^n * i}{(1+i)^n - 1}$$ Eq. 11

The levelized cost of hydrogen LCOH is then determined from the *TAC* and annual hydrogen production by:

$$\text{LCOH} = \frac{TAC}{annual\ hydrogen\ production}$$ Eq. 12

The various factors affecting the levelized cost of hydrogen (LCOH) are discussed in the results section 2.5.

2.4.1 Photovoltaic Systems

The costs of photovoltaic systems are dependent on the semi-conductor material used, the installed capacity, as well as the countries of production and installation. Furthermore, PV technology is subject to constant cost reductions due to efficiency improvements and economies of scale. These factors must be considered when evaluating the cost of photovoltaic systems. This cost can be broken down into the PV module price, the cost of the balance-of-system (BoS) components and the inverter cost. According to the photovoltaics report from the ISE Fraunhofer, the module price constituted 47%, while the BoS and inverter

cost accounted for 53% of the overall PV system investment cost in Germany for the year 2016 [44]. The installed system price for utility-scale applications, including the inverter, is set to an average of 1.25 €/Wp [44]. The PV system prices for the United States differ from those in the German market and were estimated to an average of 2.2 €/W_p for large-scale applications in 2016 by a report by the Lawrence Berkeley National Laboratory [45]. Another study from the U.S. Department of Energy estimated PV system prices in the range of around 2 €/W_p, with local deviations within the country [46]. The prices for PV systems in the United States are higher by comparison to German prices due to higher installation and BoS costs [47]. The investment costs for inverters are estimated to be 100 €/kW_p for the year 2025, according to the IRENA report [48]. The current market prices for SHJ modules, which are modeled in this study, are higher than for silicon or thin film modules. However, as silicon heterojunction is a relatively new technology in the PV market, near-term cost reductions for such modules are expected to be higher than for other PV technologies, as the effects of efficiency improvements and economies of scale are more significant. This justifies the assumption that SHJ module prices will approach those of silicon and thin film technologies against the reference year of 2025. In accordance with this assumption, the cost projection for this reference year on the basis of the average module prices, indicated above, will be adopted for the SHJ module price for the reference year 2025. The specific investment cost of the PV system in the year 2025 is set to 800 €/kWp and the O&M factor to 2% of the *CAPEX*, according to the IRENA report from 2016 [48]. The depreciation period for the PV system was assumed to last 25 years.

2.4.2 Concentrated Solar Power Generation

The commercial CSP technology can be subdivided into two dominant types of power generation, namely the parabolic trough collector (PTC) technology and solar towers (ST). Although PTC systems account for 85% of the installed CSP capacity worldwide, ST can achieve higher efficiencies, especially within the steam cycle due to higher process temperatures. In addition, the higher process temperatures favor the combination of ST technology with solid oxide electrolysis. Therefore, this study focuses on the ST technology. The economic data for investment and operational costs are derived from the IRENA report from 2015 [48]. The main contributors to the investment cost of an ST are the owner´s cost, the indirect EPC (engineering, procurement and construction) cost, thermal storage, the power block, the tower, the receiver and the solar field. In 2015, the investment cost for ST plants was 5700 €/kW installed electric capacity for a typical plant with a heat storage capacity of up to 9 h. Due to reductions in the EPC cost, investment costs are projected to decrease to 3600 €/kW_e installed electric capacity towards the year 2025. This value is used in this study. For a more detailed economic assessment, the investment cost is determined with the component cost data derived from the DLR report [49]. The investments costs of the solar tower system can be divided into three major components: that of the heliostat field, the tower and the receiver, which are 103 €/m², 72,000 €/m and 100 €/kWh_{th}, respectively. The specific thermal storage cost is 22 €/kWh, while the power block cost amounts to 1100 €/kW. The O&M factor is estimated to have been about 4% of the *CAPEX* in 2015. The projection for the year 2025

is assumed with a reduced O&M factor of 3% of *CAPEX* owing to improvements in the durability and consumption of the system over time. The lifetime of an ST plant is assumed to be 25 years.

2.4.3 Electrolysis

The current market for electrolysis systems is dominated by the highly commercialized alkaline electrolysis technology. With PEM and SOE electrolysis under further development, these technologies will steadily push into the market over the coming years to challenge the dominance of alkaline electrolysis on the basis of their beneficial operational characteristics [50].

The investment cost of PEM electrolysis systems is highly sensitive to the installed capacity. Furthermore, the reference year has an impact on the investment cost, as the PEM technology is expected to undergo rapid price reductions due to further optimization and economies of scale. Smolinka et al. determined a specific investment cost of 1200 €/kW_{Input} for mid-term development and large-scale application. The O&M factor was set to 4% of the CAPEX [50]. Bertuccioli et al. conducted a study for the Fuel Cells and Hydrogen Joint undertaking (FCH JU) that included a cost projection for PEM electrolysis. The investment cost for PEM electrolysis over the installed capacity in 2015 was indicated with 1570 €/kW_{Input} as an average over the installed capacity. The cost projection revealed an expected cost decrease to 1000 €/kW_{Input} for the year 2020 and 870 €/kW_{Input} for the year 2025 with an operational cost of 2-5% of *CAPEX* [51]. Saba et al. reviewed the literature on electrolysis costs for the last 30 years and determined a specific investment cost of 516 €/kW_{Input} for alkaline electrolysis for the year 2014, assuming an atmospheric system and installed capacity of 2.5 MW [52]. The cost gap to pressurized systems was indicated at 20%, constituting a major influence. This emphasizes the strong dependency of the investment cost on the installed capacity of the system. Large-scale applications show price reductions because auxiliary devices do not scale with the installed capacity. Mergel et al. calculated an investment cost of 585 €/kW_{Input} for the year 2013 for a large-scale PEM electrolysis system [53]. The study PlanDelyKad determined an investment cost of 363 €/$kW_{HHV\text{-}Output}$ for a 100 MW PEM electrolyzer for the reference year 2014. The operational cost in this case was assumed to be 2% of the *CAPEX* [54]. These studies share a strong dependency of the investment cost on the reference year, the nominal capacity of the system and whether or not the electrolyzer is operated under pressure. Furthermore, the assumed system efficiency determines the difference between the investment cost referenced to the input and those referenced to the output power. In this study, an investment cost of 600 €/kW_{Input} is assumed for atmospheric operation in the year 2025. The O&M factor is set to 2% of the *CAPEX.* The depreciation period *n* is 10 years, which is shorter than that of the power generation technologies because of the lower TRL of electrolysis concepts assumed here. However, within the cost sensitivity analysis in section 3.5, we have also considered a case with a 25-year depreciation time.

The SOE technology is still at the laboratory stage, with no commercial application as yet. The cost estimations and projections vary across a broad range due to the early developmental

stage of the technology. Schmidt et al. [55] conducted a survey of experts from industrial and research institutions to determine current and future costs for electrolysis technologies. They found that the expected investment cost of SOE applications would be in the range of 3000-5000 €/kW_{Input} for the year 2020. The projection for the year 2030 settled the investment cost at between 1050-4250 €/kW_{Input} [55]. These results stress the fact that cost predictions for SOE applications are dependent on the qualified estimations of experts, rather than actual market research. Based on the cost projections given above, the specific investment cost used in our study is defined with 2000 €/kW_{input} for an installed capacity of 70 MW and the reference year 2025. The O&M factor relative to *CAPEX* and the depreciation period are set to 2% and 10 years, respectively, both in analogy to the PEM electrolysis system. For the lower depreciation period, we applied the same reasoning as for PEM electrolysis. The electricity demand of auxiliary components, such as pumps, heaters, dryers and compressors is drawn from the grid. Based on recent and current values and assuming a continuous trend of reduced electricity cost for industry over time, with the electricity price for economic consideration set to 0.06 €/kWh [56].

2.4.4 Power Electronics

As mentioned above, rectifiers for the coupling of the CSP plant to the electrolysis system and DC/DC converters for the junction between the PV and the EL system are considered. According to the IRENA Report, inverters for PV systems are assumed to have an investment cost of 100 $/kW in the year 2025 [48]. The same investment cost is employed for the rectifier in this model, as these devices incorporate similar technical components. For DC/DC converters, an investment cost of 100 €/kW, an O&M factor of 2% and a depreciation period of 25 years are assumed.

2.5 Cost summary

The overall capital cost of the PV-PEM and CSP-EL pathways is determined by the sum of the subsystem's capital cost, calculated here as the annuities for each pathway. Table 5 summarizes the specific investment, operational cost rate and depreciation period per STH pathway and location considered. The shorter depreciation periods used for the PEM and SOE subsystems are discussed in section 2.4.

Table 5. Economic parameters for each technology used in this study for the base year of 2025.

Subsystem	Specific Investment cost [€/kW$_p$]	O&M [% of Investment cost]	Depreciation Period [years]
PV	800	2	25
CSP	3600	3	25
PEM	600	2	10
SOE	2000	2	10
Power Electronics	100	2	25

3 Results & Discussion

This section discusses the results of the hydrogen production predictions of all the pathways using the model-based calculations. After introducing location-specific irradiance levels, the results from optimizing the PV-based concepts of PV-PEM I and PV-PEM II for the four locations with respect to the nominal power ratio of electrolysis and PV module (see section 2.3) are presented. Based on this optimization, the nominal power and aperture area are presented, followed by the overall hydrogen production volume. Subsequently, the levelized cost of hydrogen by production concept and location are presented. A sensitivity analysis regarding the selected techno-economic parameters completes the analysis.

3.1 Location-specific irradiance levels

Figure 5 depicts the irradiance profile for Oldenburg in Germany and Daggett in the USA to exemplarily visualize the locations with the lowest and highest irradiance distribution, respectively, over the year. As can be seen for both locations, irradiation is generally higher and shows longer duration during summer days. The irradiance profiles for the other locations have similar seasonal courses over the year, but at different total irradiance levels. The respective profile representations can be found in section 5.2 of the supplementary material.

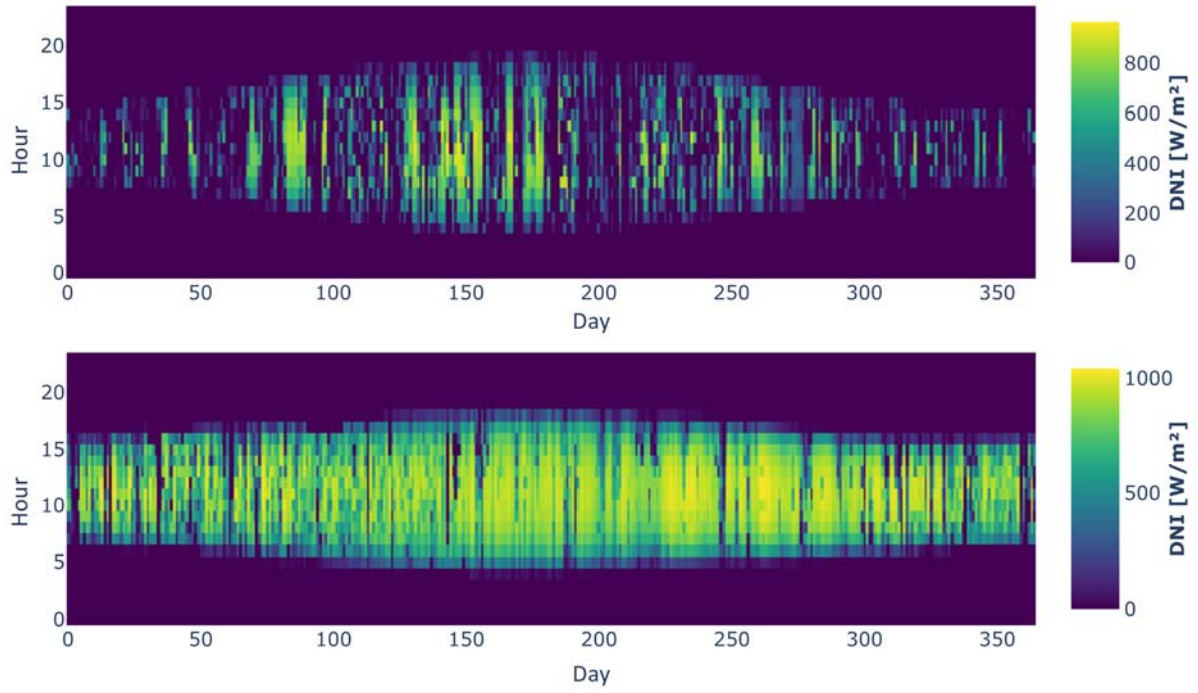

Figure 5. Irradiance profile for Oldenburg/Germany (upper) and Daggett/USA (lower).

The hourly resolved weather data irradiance and ambient temperature translate into yearly averages, which are shown in Table 6. As could be expected, the highest average irradiance was found for Daggett, followed by Almeria, Freiburg and Oldenburg. This trend is similar for the average ambient temperature with the exception of Oldenburg, which has a slightly higher value compared to Freiburg.

Table 6. Yearly averaged irradiances and ambient temperatures over one year.

Location	Average irradiance [W/m²]	Average ambient temperature [°C]
Oldenburg	259.7	11.0
Freiburg	289.4	9.7
Almeria	517.5	18.7
Daggett	525.9	19.7

3.2 Design parameters

With regard to the optimization of the PV-PEM concepts, Figure 6 depicts the hydrogen production cost for all four locations with consideration to an increasing nominal capacity ratio of EL and PV in the range of 0-100%. In general, the STH efficiency increases at higher EL- to PV-power capacity ratio because of higher electrolysis cell efficiencies, which are caused by a larger active electrolyzer area and, therefore, lower operational voltages. However, a higher active area translates into higher investment costs for the electrolyzer system. The optimum EL-PV capacity ratio is found at diverging values due to diverging irradiation characteristics per location. For Oldenburg and Freiburg, the optimum ratio is 0.5 for the PV-PEM I concept, while the optimum ratio for all of the other cases is 0.7. For the cases under

consideration, it can be concluded that in locations with higher irradiations, a higher EL-PV ratio is beneficial, as more electric power is supplied to the electrolysis system. Nevertheless, the locations of higher irradiance lead to the lowest optimized hydrogen production costs because of the higher hydrogen yield.

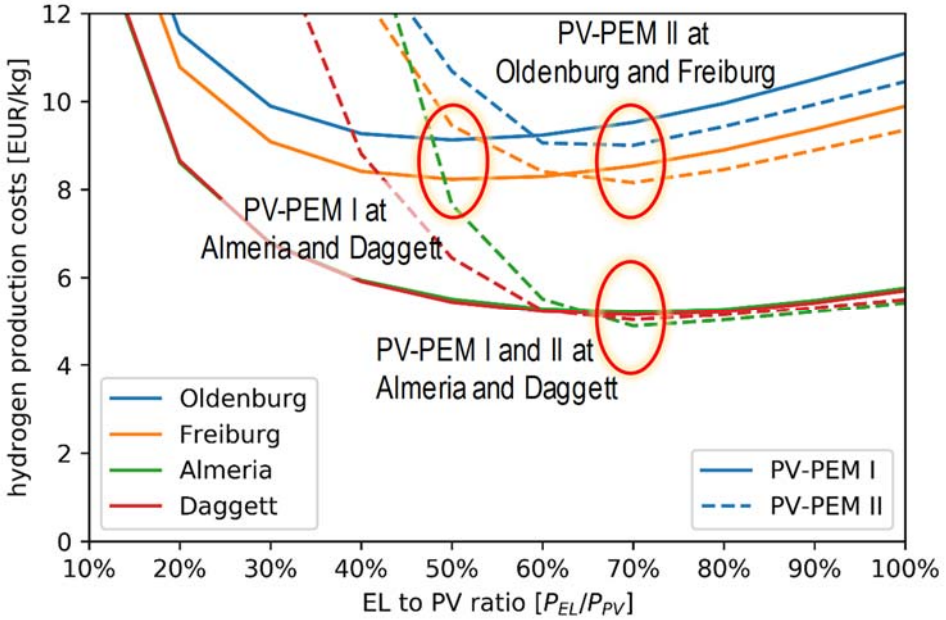

Figure 6. Optimization of the nominal power ratio of PV and EL subsystems.

Following this optimization, the electrolyzer system and power electronics have a nominal power of ca. 138 MW for Almeria and Daggett and 119 MW for Oldenburg and Freiburg. Considering the definitions related to the CSP-based concepts, Table 7 lists the nominal capacity values of the subsystems, as well as the aperture areas of all pathways.

Table 7. Nominal subsystem power and aperture areas of all pathways.

Pathways	PV/CSP [MW]	Electrolyzer [MW]		Aperture Area [km²]	
	All Locations	Almeria/Daggett	Freiburg/Oldenburg	Daggett	Almeria
CSP-SOE	70.43	70		0.91	1.12
CSP-PEM	70.43	70		0.91	1.12
PV-PEM I	205.55	138.32	119.56	1.00	
PV-PEM II	205.55	138.32	119.56	1.00	

In accordance with the different subsystems' nominal capacities, the annuity results differ by location. Related to the PV-PEM I and PV-PEM II concepts, the electrolyzer capacity differs by location and is larger in Almeria and Daggett because the irradiation at these locations is generally higher. According to the defined scope of this study, the annuity calculations for the CSP-EL concepts are carried out for Daggett and Almeria only (cf. section 2.1). Figure 7 displays site-specific investment and total annual cost (TAC) for all concepts under consideration. The related investment and TAC of the CSP-SOE pathway are highest because of the higher specific investment costs of CSP and SOE technology. Moreover, PV-PEM I

requires somewhat higher investment than PV-PEM II, as the reduced electrolyzer investment, based on the design optimization, does not fully compensate for the power converter investment.

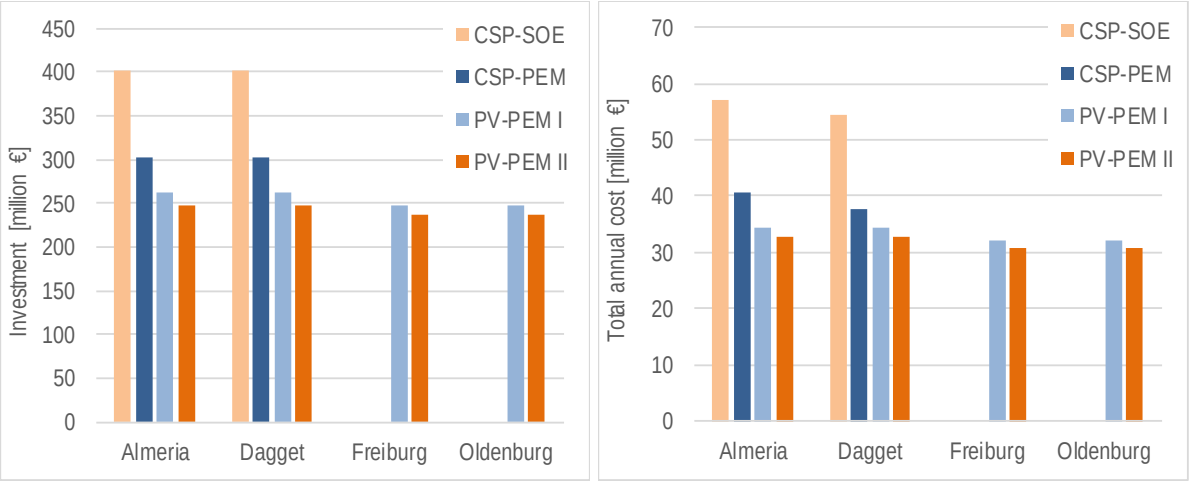

Figure 7. Investment (left) and total annual cost (right) for all concepts considered [€/a] for different locations

3.3 Hydrogen production quantity

This section presents and discusses overall hydrogen production at the locations of Oldenburg and Freiburg in Germany (PV-PEM only), as well as Almeria in Spain and Daggett in the USA (all concepts).

Figure 8 depicts the monthly hydrogen production for Oldenburg and Daggett bearing the lowest and highest hydrogen yield, respectively, of all the locations considered. The related figures for Freiburg and Almeria can be found in section 5.3 of the supplemental material. The figures clearly show a seasonal dependency of the hydrogen production quantity, highlighting an increased hydrogen production level during the summer months, which is correlated with higher irradiation during that time, as is shown in section 2.1.

The hydrogen production for the CSP-EL pathways is significantly higher than for the PV-PEM pathways. This is due to differences in the design phase. All of the pathways are designed for a solar collection area of ca. 1 km², resulting in a nominal electrical output of 70 MW_e for the CSP-EL pathways, 138 MW_e in Almeria and Daggett and 119 MW_e in Freiburg and Oldenburg for the PV-PEM I and II pathways, respectively. Although the nominal electrical output of the PV subsystems is higher, the average yearly power generation is below that of the CSP plants. This comes down to a difference in the definitions of the nominal operating points between the PV and CSP subsystems. The nominal operating point of the PV modules is equal to the maximum power point at an irradiation of 1000 W/m², while the nominal output of the CSP plants equals the average electrical output. In order to compare the pathways' competitiveness, the LCOH must be considered, as the higher total hydrogen output of the CSP-EL pathway goes in line with higher investment costs. The LCOH will be discussed in section 3.3. The hydrogen production from the pathway CSP-SOE is significantly higher across the entire year than production via the CSP-PEM pathway. This is explained by a better

electrolysis performance, as the CSP plant, power electronics and design points are equal for both pathways.

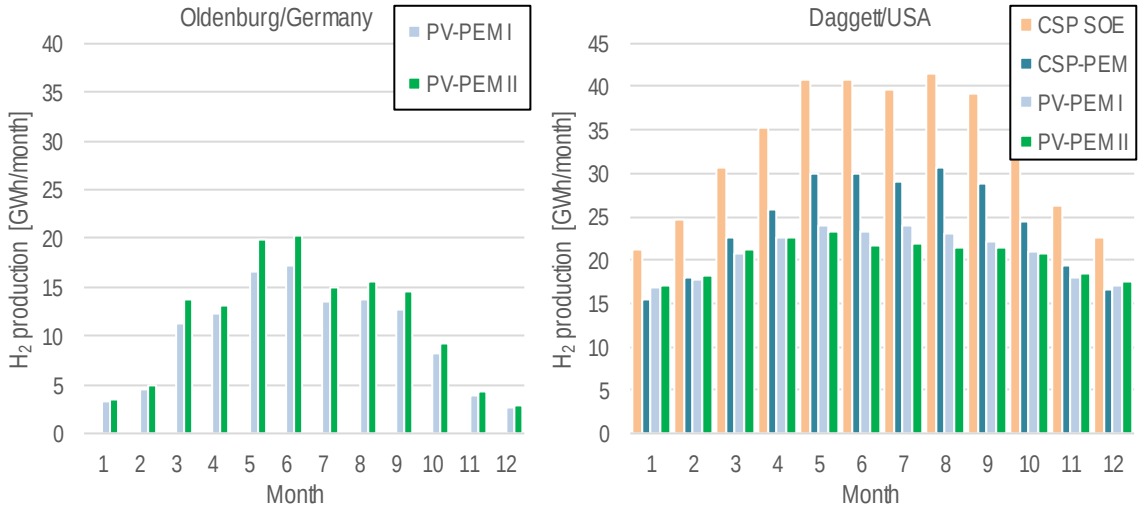

Figure 8. Monthly hydrogen production for Oldenburg (left) and Daggett (right) in the base year 2007.

Related to the PV-PEM concepts, the hydrogen production of PV-PEM I is, consistently, somewhat lower compared to PV-PEM II for the location of Oldenburg. For Daggett, there is no clear tendency; only between May and September is the H_2 yield of PV-PEM I somewhat higher compared to PV-PEM II. The expected increase caused by better coupling efficiency is not evident. Accordingly, the average STH efficiency for PV-PEM I is lower than that for PV-PEM II, with 11.2% compared to 12.8%.

Figure 9 gives an overview of total annual hydrogen production across all pathways and locations. Additionally, with the divergences between the hydrogen productions of the different pathways, the dependency on the location can be observed. From Oldenburg to Daggett, the total hydrogen production increases with average irradiation. The total STH efficiencies as the ratio of the hydrogen yield (based on the lower heating value) and irradiation *G* range from 11-13% for the PV-based concepts and 12-18% for the CSP-based ones. The highest values are found for CSP-SOE at Almeria with 16% and Daggett with 18%, which is consistent with the significantly higher hydrogen yields.

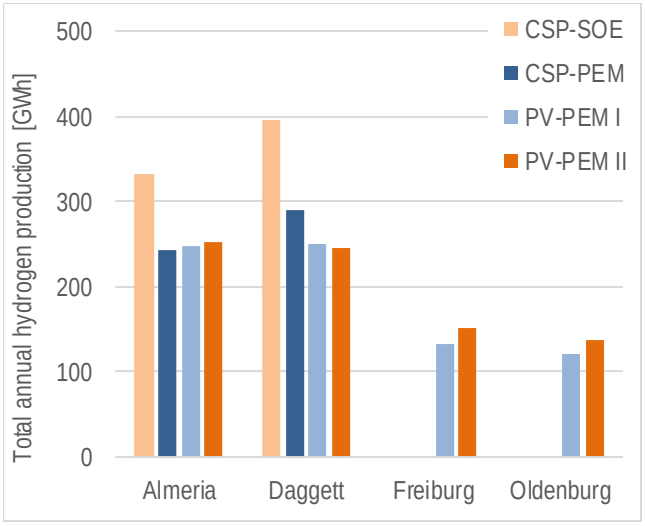

Figure 9. Total annual hydrogen production for different pathways per location using meteorological data from 2007.

3.4 Levelized cost of hydrogen

The techno-economic analysis shows the levelized cost of hydrogen for all pathways at each location; see Figure 10. The hydrogen generation cost for the locations of Oldenburg and Freiburg is nearly twice as high as the hydrogen cost in Almeria and Daggett. This reveals a direct correlation of the solar resource to the LCOH. The LCOH of the pathways PV-PEM I and PV-PEM II are nearly the same, with a very slight tendency towards lower LCOH for PV-PEM II. This shows that there is, on the one hand, no significant cost reduction achievable by coupling the subsystems PV and EL directly. Since, on the other hand, the hydrogen production volume is somewhat higher for PV-PEM II, the direct coupling has a slight advantage over coupling through a power converter.

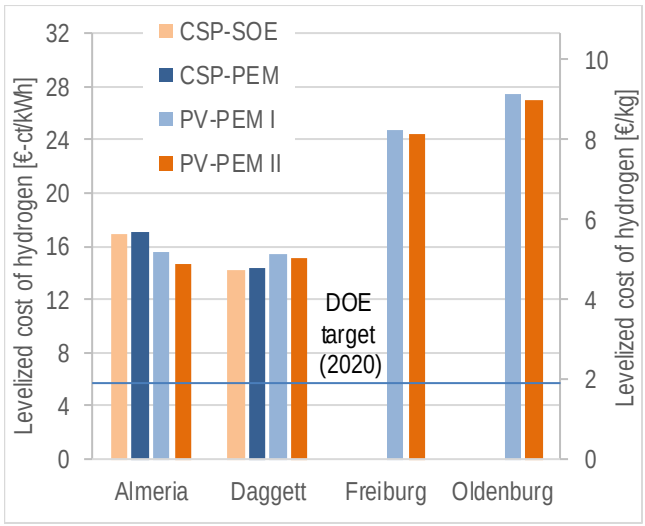

Figure 10. Levelized cost of hydrogen using costs projected for 2025 with meteorological data from 2007.

The comparison of the CSP-SOE and CSP-PEM pathways shows no cost advantage of one pathway over the other. As the hydrogen yield of the CSP-SOE concepts is significantly higher,

this concept might be the better choice. Comparing the PV-PEM and CSP-EL concepts, PV-PEM shows little lower LCOH for Almeria and little higher LCOH for Daggett, the latter featuring the higher irradiance of the two locations. Cost differences are, however, small. The cost of all four concepts range between 14 and 17 ct/kWh at the locations of Almeria and Daggett.

For the reference year 2020, the pathway-independent DOE targets for the LCOH are set with 6 $-ct/kWh. This target is only valid for hydrogen production. Within our model-based analysis, this goal could not be achieved. The lowest cost levels are derived for the CSP-PEM and CSP-SOE concepts in Daggett, with 0.14 €/kWh. The cost breakdown by concept and location shown in Figure 11 reveals, as could be expected, that the major cost drivers are power generation via PV (PV-PEM concepts) and CSP (CSP concepts), the latter having an even greater cost share of the total costs. Because of this, the effect of varied investment costs might reveal cost reduction potentials for the concepts analyzed in this study. The costs and thus cost share of the solar conversion technology, whether PV or CSP, increases for areas with lower irradiance.

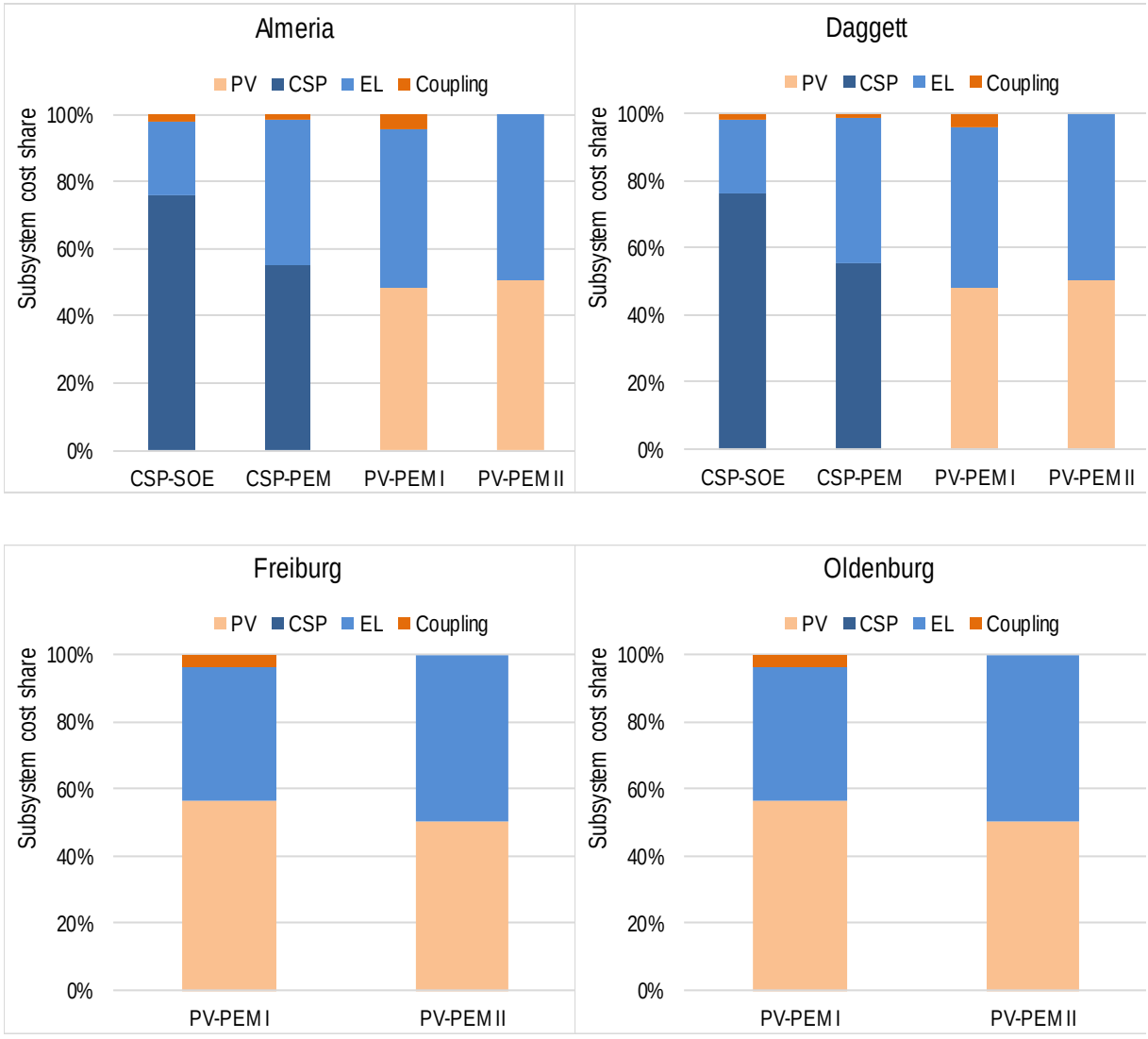

Figure 11. Break-down of contributions to the hydrogen production cost by subsystem cost.

3.5 Cost Sensitivity

As was shown above, the hydrogen cost of STH concepts are driven by the component investment. The following sensitivity analysis varies the specific investments given in Table 5 by 20% in both directions, i.e., decrease and increase. Moreover, we have chosen to vary the WACC (weighted average cost of capital) which is, in reality, subject to variation, e.g., by region and might, therefore, have a significant impact on the annual cost and total hydrogen production cost. Finally, we assume an increased depreciation period of 25 years for the electrolyzers, bringing this parameter in line with the assumptions for power generation and power conversion. The explanations below are given on the basis of the results for selected locations, namely Oldenburg (lowest irradiation levels) and Daggett (highest irradiation levels). The full set of graphic representations of our sensitivity analysis is shown in section 5.4 of the supplemental material.

The results of our sensitivity analysis relating to the location of Oldenburg are displayed in Figure 12. A decreased PV investment and WACC would reduce the hydrogen cost by 10% and 8%, respectively. Also, for these concepts an increased depreciation period of 25 years would be highly beneficial with a 12% (PV-PEM I) and 13% (PV-PEM-II) cost decrease, respectively.

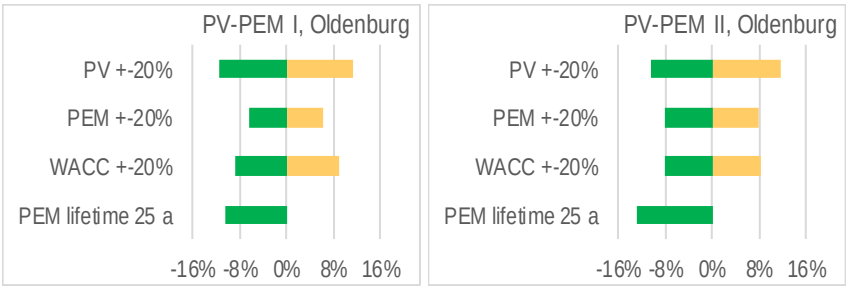

Figure 12. Cost sensitivities of the PV-PEM I and PV-PEM II concepts for the example of Oldenburg/Germany.

Figure 13 shows the results of the respective sensitivity analysis related to the two CSP-EL concepts at the location of Daggett. The impact of the selected parameters on the LCOH ranges between 8% and 15%. For the CSP-SOE concept, the lifetime extension has the greatest impact with 14%, followed by the reduction of CSP investment with 11%. The latter also has the most significant impact on the CSP-PEM concept with 15%. The second is the WACC which, if reduced, would decrease the cost of hydrogen by 9%. Lifetime expansion is also the most significant for PV-PEM II.

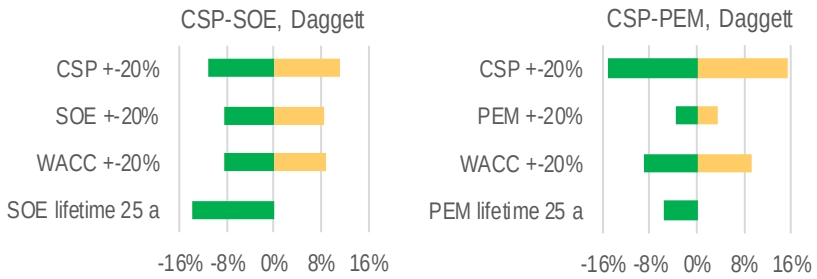

Figure 13. Cost sensitivities of the CSP-SOE and CSP-PEM concepts for the example of Daggett/USA.

Our results also show that of all the pathway power generation technologies, CSP and PV have a higher impact on the LCOH than the electrolysis technologies.

3.6 Cost Reduction Potential

In the final step of our cost assessment, we combine the individual assumptions aimed at reducing costs to identify an overall cost reduction potential for the concepts considered in this study.

The results of combining the cost reduction factors considered are shown for the CSP-SOE concept in Figure 14. It can be seen that the hydrogen production cost could be reduced to a level of 9-11 €-ct/kWh (3.00-3.67 €/kg$_{H2}$) for Almeria and Daggett if it was possible to reduce the investment costs of the CSP and SOE by 20%, extend the depreciation period of SOE to 25 years and if a reduced WACC of 6.4% would be applicable. The respective costs for the CSP-PEM (see section 5.5 in the supplemental material) would be slightly elevated to 10-12 €-ct/kWh (3.33-4.00 €/kg$_{H2}$).

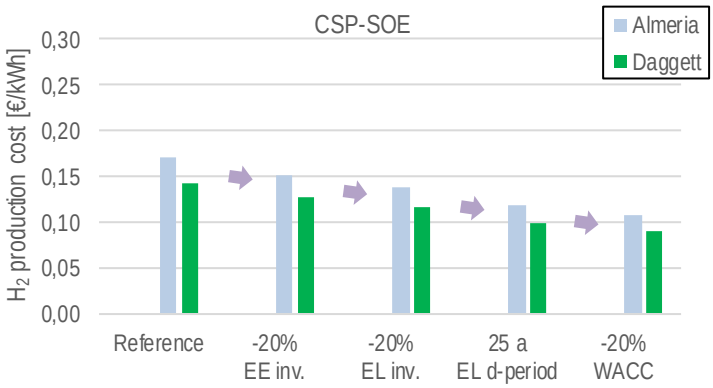

Figure 14. Cost reduction potential of the CSP-SOE concept with the energy conversion efficiency unchanged.

Related to the PV-PEM I concept, our analysis reveals similar cost levels of 10 €-ct/kWh (3.33 €/kg$_{H2}$) under our most optimistic assumptions for Almeria and Daggett. Due to significantly lower irradiation levels in Oldenburg and Freiburg, the cost level is higher, at 16-18 €-ct/kWh (5.33-6.00 €/kg$_{H2}$).

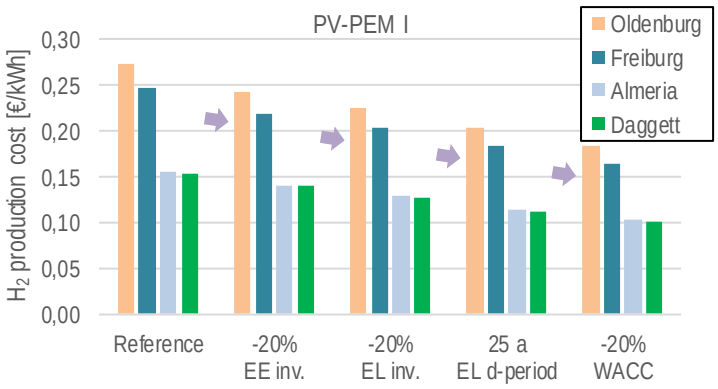

Figure 15. Cost reduction potential of the PV-PEM I concept with the energy conversion efficiency unchanged.

4 Conclusions

In this paper, candidate concepts of solar-based, electrolytic hydrogen production (solar-to-hydrogen, STH) were analyzed. On the power provision side, photovoltaic and concentrated solar power systems were considered. These options are combined with electrolytic hydrogen production alternatives of PEM electrolysis with (PV-PEM I and CSP-PEM) or without (PV-PEM II) power converters for electric coupling. Additionally, a concept including CSP and solid oxide electrolysis coupled via a power converter (CSP-SOE) has been considered for evaluating the effect of integrating heat from the CSP process into high-temperature electrolysis. A TRL analysis of the sub-components revealed that the highest pathway TRL levels can be estimated for the PV- and CSP-based power generation, coupled to a PEM electrolysis system, due to the high maturity of subsystems. Low TRL was found for systems comprising SOE technology. Photo-electrochemical water-splitting is not further explored within the model, as the low TRL of this technology does not promise near-term economic feasibility.

The developed techno-economic model was applied to determine hydrogen production volumes and the levelized cost of hydrogen (LCOH) at the locations of Oldenburg and Freiburg in Germany, as well as Almeria in Spain and Daggett in the USA, employing location-specific irradiation and ambient temperature data. Due to comparatively low irradiation levels in Germany, CSP-based systems have not been considered here. All cost data was projected for the reference year 2025.

The lowest LCOH of 14 €-ct/kWh$_{H2}$ was found for the CSP-SOE and CSP-PEM pathways in Daggett. At reduced irradiation levels in Almeria, these pathways show an LCOH increase of 19%. The LCOH of the PEM-based pathways are slightly elevated, with values ranging from 15-16 €-ct/kWh$_{H2}$ for both high-irradiance locations. For the two locations in Germany, the LCOH related to the PV-PEM concepts is 58-84% higher compared to the locations of Almeria and Daggett due to the considerably lower irradiation levels. Our analysis reveals that there is no significant cost effect of applying power converters for connecting PV modules and PEM electrolysis. We conclude that a theoretically increased hydrogen production volume through the employment of a power converter is not evident because the cost-optimization procedure leads to a lower electrolyzer capacity, which in turn reduces hydrogen production volumes.

Furthermore, our analysis shows that the cost-competitiveness of CSP-EL compared to PV-PEM concepts increases with irradiation levels.

LCOH differences of CSP-SOE compared to CSP-PEM are found to be small and may be within computational error tolerances. However, CSP-SOE shows substantially higher hydrogen production levels of 36%relative to CSP-PEM at both of the locations considered. Hence, STH efficiencies are also highest, with 16-18%, at the locations of Almeria and Daggett.

The LCOH values achieved by the solar-to-hydrogen concepts considered in this study at the parameter settings chosen and with regard to an expected capital cost level in 2025 were still significantly higher than the DOE's 2020 targets for economically-viable hydrogen production of 6 $-ct/kWh. However, if it was possible to further reduce component and capital costs by 20% and also achieve depreciation periods of 25 years for electrolyzers, the LCOH would range from 9-12 €-ct/kWh_{H2} for the high-irradiance locations and, thus, would be closer to the DOE targets.

In relation to future research, a further system optimization is suggested regarding the implementation of short-term energy storage, which might be particularly relevant at locations with higher fluctuations in power supply.

Conflicts of interest

There are no conflicts of interest to be declared.

Acknowledgements

This work was supported by the Helmholtz Association under the Joint Initiative "EnergySystem 2050 – A Contribution of the Research Field Energy".

Nomenclature

a	Modified ideality factor
A_{EL}	Active electrode area of the electrolyzer
AM	Air mass
e	Elementary charge
EL	Electrolysis
G	Solar irradiation
G_{design}	Design irradiance
HER	Hydrogen evolution reaction
I_0	Diode reverse saturation current
I_{MPP}	Current at MPP
I_{ph}	Photo current
I_{SC}	Short circuit current
J_{nom}	Current density at nominal operating point of electrolyzer
LCOE	Levelized cost of electricity
MPP	Maximum power point of a photovoltaic module
NREL	National Renewable Energy Laboratory (USA)
OER	Oxygen evolution reaction
PEC	Photoelectrolysis
PEM	Polymer electrolyte membrane
Pt	Platinum
P_{MPP}	Power at MPP
PV	Photovoltaic
PV-EL	Coupled photovoltaic electrolysis system
U_{MPP}	Voltage at MPP
U_{nom}	Voltage at nominal operation point of electrolyzer
U_{OC}	Open circuit voltage
R_p	Shunt resistance
R_s	Series resistance
SAM	System advisor module
SHJ	Silicon heterojunction technology
STH	Solar-to-hydrogen
T_{amb}	Ambient temperature
T_{EL}	Electrolysis temperature
T_{PV}	Cell temperature of the PV subsystem
T_{op}	Operating temperature of the electrolyte
TiO_2	Titanium dioxide
η	Efficiency

References

1. Otto, A., M. Robinius, T. Grube, S. Schiebahn, A. Praktiknjo, and D. Stolten, *Power-to-Steel: Reducing CO2 through the Integration of Renewable Energy and Hydrogen into the German Steel Industry.* Energies, 2017. **10**(4): p. 451.
2. Robinius, M., A. Otto, P. Heuser, L. Welder, K. Syranidis, D. Ryberg, T. Grube, P. Markewitz, R. Peters, and D. Stolten, *Linking the Power and Transport Sectors—Part 1: The Principle of Sector Coupling.* Energies, 2017. **10**(7): p. 956.
3. Robinius, M., A. Otto, K. Syranidis, D.S. Ryberg, P. Heuser, L. Welder, T. Grube, P. Markewitz, V. Tietze, and D. Stolten, *Linking the Power and Transport Sectors—Part 2: Modelling a Sector Coupling Scenario for Germany.* Energies, 2017. **10**(7): p. 957.

4. Reuß, M., J. Reul, T. Grube, M. Langemann, S. Calnan, M. Robinius, R. Schlatmann, U. Rau, and D. Stolten, *Solar hydrogen production: a bottom-up analysis of different photovoltaic–electrolysis pathways.* Sustainable Energy & Fuels, 2019.
5. Clarke, R.E., S. Giddey, F.T. Ciacchi, S.P.S. Badwal, B. Paul, and J. Andrews, *Direct coupling of an electrolyser to a solar PV system for generating hydrogen.* International Journal of Hydrogen Energy, 2009. **34**(6): p. 2531-2542.
6. Heremans, G., C. Trompoukis, N. Daems, T. Bosserez, I.F.J. Vankelecom, J.A. Martens, and J. Rongé, *Vapor-fed solar hydrogen production exceeding 15% efficiency using earth abundant catalysts and anion exchange membrane.* Sustainable Energy Fuels, 2017.
7. Su, Z., S. Ding, Z. Gan, and X. Yang, *Analysis of a photovoltaic-electrolyser direct-coupling system with a V-trough concentrator.* Energy Conversion and Management, 2016. **108**: p. 400-410.
8. Turner, J., G. Sverdrup, M.K. Mann, P.-C. Maness, B. Kroposki, M. Ghirardi, R.J. Evans, and D. Blake, *Renewable hydrogen production.* International Journal of Energy Research, 2008. **32**(5): p. 379-407.
9. T. Jesper Jacobsson, V.F., Marika Edoff, Tomas Edvinsson *Sustainable solar hydrogen production: from photoelectrochemical cells to PV-electrolyzers and back again.* Energy & Environmental Science, 2014.
10. Dincer, I. and C. Acar, *Review and evaluation of hydrogen production methods for better sustainability.* International Journal of Hydrogen Energy, 2015. **40**(34): p. 11094-11111.
11. Acar, C. and I. Dincer, *Comparative assessment of hydrogen production methods from renewable and non-renewable sources.* International Journal of Hydrogen Energy, 2014. **39**(1): p. 1-12.
12. Dincer, I., *Green methods for hydrogen production.* International Journal of Hydrogen Energy, 2012. **37**(2): p. 1954-1971.
13. Kibria, M.G. and Z. Mi, *Artificial photosynthesis using metal/nonmetal-nitride semiconductors: current status, prospects, and challenges.* J. Mater. Chem. A, 2016. **4**(8): p. 2801-2820.
14. Sayedin, F., A. Maroufmashat, S. Sattari, A. Elkamel, and M. Fowler, *Optimization of Photovoltaic Electrolyzer Hybrid systems; taking into account the effect of climate conditions.* Energy Conversion and Management, 2016. **118**: p. 438-449.
15. Sayedin, F., A. Maroufmashat, R. Roshandel, and S.S. Khavas, *Optimal design and operation of a photovoltaic–electrolyser system using particle swarm optimisation.* International Journal of Sustainable Energy, 2016. **35**(6): p. 566-582.
16. Sayedin, F., A. Maroufmashat , S. Al-Adwani, S. Sattari, A. Elkamel, and M. Fowler, *Evolutionary Optimization Approaches for Direct Coupling Photovoltaic-Electrolyzer*

Systems. Industrial Engineering and Operations Management (IEOM), 2015 International Conference on, 2015.

17. Garciavalverde, R., C. Miguel, R. Martinezbejar, and A. Urbina, *Optimized photovoltaic generator–water electrolyser coupling through a controlled DC–DC converter.* International Journal of Hydrogen Energy, 2008. **33**(20): p. 5352-5362.
18. García-Valverde, R., N. Espinosa, and A. Urbina, *Optimized method for photovoltaic-water electrolyser direct coupling.* International Journal of Hydrogen Energy, 2011. **36**(17): p. 10574-10586.
19. Barbir, F. and T.N. Veziroglu, *Solar–Hydrogen Energy System: The Choice of the Future.* Int. J. Hydrogen Energy, 2009.
20. Kirner, S., P. Bogdanoff, B. Stannowski, R. van de Krol, B. Rech, and R. Schlatmann, *Architectures for scalable integrated photo driven catalytic devices-A concept study.* International Journal of Hydrogen Energy, 2016. **41**(45): p. 20823-20831.
21. Pinaud, B.A., J.D. Benck, L.C. Seitz, A.J. Forman, Z. Chen, T.G. Deutsch, B.D. James, K.N. Baum, G.N. Baum, S. Ardo, H. Wang, E. Miller, and T.F. Jaramillo, *Technical and economic feasibility of centralized facilities for solar hydrogen production via photocatalysis and photoelectrochemistry.* Energy & Environmental Science, 2013. **6**(7): p. 1983-2002.
22. Shaner, M.R., H.A. Atwater, N.S. Lewis, and E.W. McFarland, *A comparative technoeconomic analysis of renewable hydrogen production using solar energy.* Energy Environ. Sci., 2016. **9**(7): p. 2354-2371.
23. Dumortier, M., S. Tembhurne, and S. Haussener, *Holistic design guidelines for solar hydrogen production by photo-electrochemical routes.* Energy Environ. Sci., 2015. **8**(12): p. 3614-3628.
24. Dumortier, M. and S. Haussener, *Design guidelines for concentrated photo-electrochemical water splitting devices based on energy and greenhouse gas yield ratios.* Energy Environ. Sci., 2015. **8**(11): p. 3069-3082.
25. Roeb, M., N. Monnerie, A. Houaijia, D. Thomey, and C. Sattler, *Chapter 4 - Solar Thermal Water Splitting A2 - Gandía, Luis M*, in *Renewable Hydrogen Technologies*, G. Arzamendi and P.M. Diéguez, Editors. 2013, Elsevier: Amsterdam. p. 63-86.
26. Mankins, J.C., *Technology Readiness Level*, 1995.
27. E.U., *Horizon 2020 – Work Programme*, 2014.
28. Kopp, M., D. Coleman, C. Stiller, K. Scheffer, J. Aichinger, and B. Scheppat, *Energiepark Mainz: Technical and economic analysis of the worldwide largest Power-to-Gas plant with PEM electrolysis.* International Journal of Hydrogen Energy, 2017.
29. *Typical Meteorological Year Data*, 2017, European Commission and Joint Research Centre (JRC).
30. *System Advisor Model (SAM)*, 2017, National Renewable Energy Laboratory: Golden, CO.

31. Tamrakar, V., G. S.C, and Y. Sawle, *Single-Diode and Two-Diode Pv Cell Modeling Using Matlab For Studying Characteristics Of Solar Cell Under Varying Conditions.* Electrical & Computer Engineering: An International Journal, 2015. **4**(2): p. 67-77.
32. De Soto, W., S.A. Klein, and W.A. Beckman, *Improvement and validation of a model for photovoltaic array performance.* Solar Energy, 2006. **80**(1): p. 78-88.
33. Dunn, R.I., P.J. Hearps, and M.N. Wright, *Molten-Salt Power Towers: Newly Commercial Concentrating Solar Storage.* Proceedings of the IEEE, 2012. **100**(2): p. 504-515.
34. Dersch, J. and S. Dieckmann, *greenius - The Green Energy System Analysis Tool*, 2019, German Aerospace Center: Cologne.
35. NREL. *System Advisor Model (SAM)*. 2017 [cited 2017; Available from: https://sam.nrel.gov/.
36. Klotz, D., A. Leonide, A. Weber, and E. Ivers-Tiffée, *Electrochemical model for SOFC and SOEC mode predicting performance and efficiency.* International Journal of Hydrogen Energy, 2014. **39**(35): p. 20844-20849.
37. Fang, Q., L. Blum, and N.H. Menzler, *Performance and Degradation of Solid Oxide Electrolysis Cells in Stack.* Journal of the Electrochemical Society, 2015. **162**(8): p. F907-F912.
38. Peters, R., R. Deja, L. Blum, V.N. Nguyen, Q. Fang, and D. Stolten, *Influence of operating parameters on overall system efficiencies using solid oxide electrolysis technology.* International Journal of Hydrogen Energy, 2015. **40**(22): p. 7103-7113.
39. Nguyen, V.N., Q. Fang, U. Packbier, and L. Blum, *Long-term tests of a Jülich planar short stack with reversible solid oxide cells in both fuel cell and electrolysis modes.* International Journal of Hydrogen Energy, 2013. **38**(11): p. 4281-4290.
40. *Hydrogen Science and Engineering: Materials, Processes, Systems and Technology*2016: Wiley-VCH Verlag GmbH & Co. KGaA.
41. Tjarks, G., *PEM-Elektrolyse-Systeme zur Anwendung in Power-to-Gas Anlagen*, 2017, RWTH Aachen University.
42. Tjarks, G., A. Gibelhaus, F. Lanzerath, M. Müller, A. Bardow, and D. Stolten, *Energetically-optimal PEM electrolyzer pressure in power-to-gas plants.* Applied Energy, 2018. **218**: p. 192-198.
43. Nordmann, S., B. Berghoff, A. Hessel, N. Wilck, B. Osullivan, M. Debucquoy, J. John, S. Starschich, and J. Knoch, *A monolithic all-silicon multi-junction solar device for direct water splitting.* Renewable Energy, 2016. **94**: p. 90-95.
44. Fraunhofer, I., *Photovoltaics Report*, 2017, ISE Fraunhofer.
45. Bolinger, M., J. Seel, and K. LaCommare, *Empirical Analysis of Project Cost, Performance, and Pricing*, 2017, Lawrence Berkeley National Laboratory.

46. Feldman, D., R. Margolis, M. Bolinger, D. Chung, R. Fu, J. Seel, G. Barbose, C. Davidson, N. Darghouth, and R. Wiser, *Photovoltaic System Pricing Trends*, 2015, U.S Department of Energy.
47. Seel, J., G. Barbose, and R. Wiser, *Why Are Residential PV Prices in Germany So Much Lower Than in the United States?*, 2013, Lawrence Berkeley National Laboratory.
48. *The Power to Change : Solar and Wind Cost Reduction Potential to 2025*2016: The International Renewable Energy Agency (IRENA).
49. Dieckmann, S., J. Dersch, S. Giuliano, M. Puppe, E. Lüpfert, K. Hennecke, R. Pitz-Paal, M. Taylor, and P. Ralon. *LCOE Reduction Potential of Parabolic Trough and Solar Tower CSP Technology until 2025*. in *SolarPACES Conference*. 2016. Abu Dhabi: DLR.
50. Smolinka, T., M. Günther, and J. Garche, *NOW-Studie: Stand und Entwicklungspotenzial der Wasserelektrolyse zur Herstellung von Wasserstoff aus regenerativen Energien*, 2011, Fraunhofer ISE.
51. Bertuccioli, L., A. Chan, D. Hart, F. Lehner, B. Madden, and E. Standen, *Development of Water Electrolysis in the European Union - Final Report*, 2014, E4tech Sàrl/element energy: Lausanne/Cambridge.
52. Saba, S.M., M. Müller, M. Robinius, and D. Stolten, *The investment costs of electrolysis – A comparison of cost studies from the past 30 years.* International Journal of Hydrogen Energy, 2017.
53. Jürgen Mergel, M.C., David Fritz, *Status on Technologies for Hydrogen Production by Water Electrolysis*, in *Transition to Renewable Energy Systems*2013.
54. Fraunhofer, I., *PlanDelyKad: Studie über die Planung einer Demonstrationsanlage zur Wasserstoff-Kraftstoffgewinnung durch Elektrolyse mit Zwischenspeicherung in Salzkavernen unter Druck*, 2014, ISE Fraunhofer, Ludwig-Bölkow-Systemtechnik, DLR Stuttgart.
55. Schmidt, O., A. Gambhir, I. Staffell, A. Hawkes, J. Nelson, and S. Few, *Future cost and performance of water electrolysis: An expert elicitation study.* International Journal of Hydrogen Energy, 2017. **42**(52): p. 30470-30492.
56. *Prices of electricity for the industry in Germany from 2008 to 2018*. 22.04.2020]; Available from: https://www.statista.com/statistics/595803/electricity-industry-price-germany/. .
57. *International Technology Roadmap for Photovoltaic*, 2015.
58. Publicover, B., *JinkoSolar claims new 22.78% PERC efficiency record*, in *PV Magazine*2017.
59. Solar, L., *Conversion Efficiency at 20.41%, LONGi Solar Creates World Record of Monocrystalline PERC Module*, 2018.

60. *New World Record Established for Conversion Efficiency in a Crystalline Silicon Solar Cell*, 2017, Kaneka Corporation.
61. Corporation, K., *World's Highest Conversion Efficiency of 24.37% Achieved in a Crystalline Silicon Solar Cell Module*, 2017.
62. *26.1% record efficiency for p-type crystalline Si solar cells*. 2018 [cited 2018 06 Feb]; Available from: https://isfh.de/en/26-1-record-efficiency-for-p-type-crystalline-si-solar-cells/.
63. Zeng, K. and D. Zhang, *Recent progress in alkaline water electrolysis for hydrogen production and applications.* Progress in Energy and Combustion Science, 2010. **36**(3): p. 307-326.
64. Holladay, J.D., J. Hu, D.L. King, and Y. Wang, *An overview of hydrogen production technologies.* Catalysis Today, 2009. **139**(4): p. 244-260.
65. Manabe, A., M. Kashiwase, T. Hashimoto, T. Hayashida, A. Kato, K. Hirao, I. Shimomura, and I. Nagashima, *Basic study of alkaline water electrolysis.* Electrochimica Acta, 2013. **100**: p. 249-256.
66. Barisic, M., *Alkalische Elektrolyse in der Industriellen Anwendung*, 2012, ELB Elektrolysetechnik.
67. Chakik, F.e., M. Kaddami, and M. Mikou, *Effect of operating parameters on hydrogen production by electrolysis of water.* International Journal of Hydrogen Energy, 2017. **42**(40): p. 25550-25557.
68. Babic, U., M. Suermann, F.N. Büchi, L. Gubler, and T.J. Schmidt, *Critical Review—Identifying Critical Gaps for Polymer Electrolyte Water Electrolysis Development.* Journal of The Electrochemical Society, 2017. **164**(4): p. F387-F399.
69. Ganley, J.C., *High temperature and pressure alkaline electrolysis.* International Journal of Hydrogen Energy, 2009. **34**(9): p. 3604-3611.
70. Allebrod, F., C. Chatzichristodoulou, and M.B. Mogensen, *Alkaline electrolysis cell at high temperature and pressure of 250 °C and 42 bar.* Journal of Power Sources, 2013. **229**: p. 22-31.
71. Bhandari, R., C.A. Trudewind, and P. Zapp, *Life cycle assessment of hydrogen production via electrolysis – a review.* Journal of Cleaner Production, 2014. **85**: p. 151-163.
72. Olivier, P., C. Bourasseau, and P.B. Bouamama, *Low-temperature electrolysis system modelling: A review.* Renewable and Sustainable Energy Reviews, 2017. **78**: p. 280-300.
73. Carmo, M., D.L. Fritz, J. Mergel, and D. Stolten, *A comprehensive review on PEM water electrolysis.* International Journal of Hydrogen Energy, 2013. **38**(12): p. 4901-4934.
74. Chandesris, M., R. Vincent, L. Guetaz, J.S. Roch, D. Thoby, and M. Quinaud, *Membrane degradation in PEM fuel cells: From experimental results to semi-empirical*

degradation laws. International Journal of Hydrogen Energy, 2017. **42**(12): p. 8139-8149.

75. Ozden, E. and I. Tari, *PEM fuel cell degradation effects on the performance of a stand-alone solar energy system.* International Journal of Hydrogen Energy, 2017. **42**(18): p. 13217-13225.
76. Ayers, K.E., J.N. Renner, N. Danilovic, J.X. Wang, Y. Zhang, R. Maric, and H. Yu, *Pathways to ultra-low platinum group metal catalyst loading in proton exchange membrane electrolyzers.* Catalysis Today, 2016. **262**: p. 121-132.
77. Whitney G. Colella, B.D.J., Jennie M. Moton, Genevieve Saur, Todd Ramsden, *Techno-economic Analysis of PEM Electrolysis for Hydrogen Production.* 2014.
78. Bensmann, B., R. Hanke-Rauschenbach, and K. Sundmacher, *In-situ measurement of hydrogen crossover in polymer electrolyte membrane water electrolysis.* International Journal of Hydrogen Energy, 2014. **39**(1): p. 49-53.
79. Schalenbach, M., M. Carmo, D.L. Fritz, J. Mergel, and D. Stolten, *Pressurized PEM water electrolysis: Efficiency and gas crossover.* International Journal of Hydrogen Energy, 2013. **38**(35): p. 14921-14933.
80. Tietz, F., D. Sebold, A. Brisse, and J. Schefold, *Degradation phenomena in a solid oxide electrolysis cell after 9000 h of operation.* Journal of Power Sources, 2013. **223**(Supplement C): p. 129-135.
81. Chatzichristodoulou, C., M. Chen, P.V. Hendriksen, T. Jacobsen, and M.B. Mogensen, *Understanding degradation of solid oxide electrolysis cells through modeling of electrochemical potential profiles.* Electrochimica Acta, 2016. **189**(Supplement C): p. 265-282.
82. Schiller, G., M. Hörlein, and A. Nechache, *Detailed Study of Degradation Behavior of Solid Oxide Cells in Electrolysis and Co-Electrolysis Mode*, 2016, German Aerospace Center (DLR).
83. http://www.solarpaces.org/how-csp-works/. 09.03.2018].
84. Barlev, D., R. Vidu, and P. Stroeve, *Innovation in concentrated solar power.* Solar Energy Materials and Solar Cells, 2011. **95**(10): p. 2703-2725.
85. Romero, M. and A. Steinfeld, *Concentrating solar thermal power and thermochemical fuels.* Energy & Environmental Science, 2012. **5**(11): p. 9234.
86. Dunn, R.I., P.J. Hearps, and M.N. Wright., *Molten-salt power towers: newly commercial concentrating solar storage*, in *IEEE*2012.
87. R. C. Kainthla, B.Z., J. O'M. Bockris, *Significant efficiency increase in self-driven photoelectrochemical cell for water photoelectrolysis.* Journal of the Electrochemical Society, 1987. **134** (4): p. 841-845.
88. Artiphyction. *Fully artificial photo-electrochemical device for low temperature hydrogen production*. 2018 [cited 2018 12 Feb]; Available from: http://www.artiphyction.org.

89. Kim, J.H., Y. Jo, J.H. Kim, J.W. Jang, H.J. Kang, Y.H. Lee, D.S. Kim, Y. Jun, and J.S. Lee, *Wireless Solar Water Splitting Device with Robust Cobalt-Catalyzed, Dual-Doped BiVO4 Photoanode and Perovskite Solar Cell in Tandem: A Dual Absorber Artificial Leaf.* ACS Nano, 2015. **9**(12): p. 11820-11829.

90. Kim, J.H., J.-W. Jang, Y.H. Jo, F.F. Abdi, Y.H. Lee, R. van de Krol, and J.S. Lee, *Hetero-type dual photoanodes for unbiased solar water splitting with extended light harvesting.* Nature Communications, 2016. **7**(1): p. 13380.

91. Walczak, K.A., G. Segev, D.M. Larson, J.W. Beeman, F.A. Houle, and I.D. Sharp, *Hybrid Composite Coatings for Durable and Efficient Solar Hydrogen Generation under Diverse Operating Conditions.* Advanced Energy Materials, 2017. **7**(13): p. 1602791.

92. Becker, J.P., B. Turan, V. Smirnov, K. Welter, F. Urbain, J. Wolff, S. Haas, and F. Finger, *A modular device for large area integrated photoelectrochemical water-splitting as a versatile tool to evaluate photoabsorbers and catalysts.* J. Mater. Chem. A, 2017.

5 Supplemental Material

5.1 State-of-the-Art and TRL of Subsystems

5.1.1 Photovoltaic Devices and Modules

Electricity generation by solar cells using the photovoltaic effect has already achieved the highest technology level of TRL 9. Commercially-mature products have been on the market for more than a decade. Although numerous PV technologies exist, classified chiefly by the absorber material, the following discussion shall cover only the state-of-the art as far as commercially-available PV technologies are concerned. Crystalline silicon-based solar cells have the largest market share of PV modules. Within this technology path, p-type multi-crystalline silicon, using a combination of diffused junctions and a back surface field, predominate [57]. While the typical efficiency of commercial cells does not exceed 19%, a record efficiency of 22% was achieved for a 246 cm² multi-crystalline p-type silicon single wafer using passivated emitter rear cell (PERC) technology [58]. The highest present module efficiency of 20.4% has been reported for p-type mono-crystalline silicon, also based on PERC technology [59]. Even higher efficiencies have been achieved using n-type mono-crystalline silicon, which is believed to have a higher intrinsic efficiency limit than p-type silicon. At the time of writing this paper, the highest silicon efficiency values of 26.6% are reported for a 180 cm² single cell wafer [60] and 24.4% for a module with an area of 1.3 m² [61]. Here, the silicon heterojunction (SHJ) technology on n-type mono-crystalline silicon is used. Solar cells based on this technology are available on the market with efficiencies above 19.5% (see section 3.2.1). The recently reported efficiency record for small area solar cells based on p-type mono-crystalline silicon of 26.1% (4 cm²) [62] comes close to the highest efficiency values reported on a 180 cm² single cell wafer of 26.6% [60]. In summary, recent innovations in the PV device field have caused a growth in the market share of modules using mono-crystalline silicon because falling manufacturing cost have increased the effect of an efficiency gain on the levelized cost of electricity (LCOE) [57]. Moreover, higher efficiency values reduce the specific cost of the balance of system and, at the same time, increase the power output for the same module area. Thus, it is expected that PV-based STH efficiency is expected to increase and the cost will be reduced.

5.1.2 Electrolysis

The field of water electrolysis can be subdivided into three major technology pathways. Alkaline electrolysis is the most common technology with the highest market share and longest history of development [63, 64, 65]. There are installed systems with a nominal power exceeding 1 MW and system efficiencies of up to 80% (higher heating value) [66, 67]. A typical specific investment for this technology is reported to be 1100 $/kW [50, 68]. Due to the high maturity of alkaline electrolysis systems, the TRL can be defined with a value of 9. Pressurized electrolysis and operation at elevated temperature is considered to further improve the efficiency of alkaline electrolysis systems [69, 70]. Polymer electrolyte membrane (PEM),

electrolysis, meanwhile, is the most anticipated technology for future applications. This is due to expected cost reductions, decreasing specific investment to 500 $/kW and below as well as system efficiencies exceeding 80% (higher heating value) [28, 71, 72]. Specific investment costs at present are still in the range of 2000 $/kW due to small market penetration [50, 68, 73]. There have been numerous setups demonstrating the technology at a nominal power level of several kW. Recently, this scale has been pushed by the launch of the Energiepark Mainz, which utilizes a PEM electrolyzer with a nominal output of 6 MW [28]. On the basis of this progress, the TRL of PEM technology can be estimated to be 8. Current research in the field of PEM electrolysis focuses on technological progress to achieve industrial readiness. This includes improved lifetime and durability of PEM stacks by investigating degradation mechanisms [74, 75]. Moreover, reduced catalyst-loading and gas-crossover through the membrane, increased system pressure as well as cost reductions through increased manufacturing volume are targets of current development efforts [68, 73, 76, 77, 78, 79]. Solid oxide electrolysis cells (SOE) operate at high-temperatures of between 600-900°C with higher system efficiencies than PEM electrolyzers, depending on how much waste heat from nearby processes can be integrated [36, 37, 38]. Currently, no commercial applications have been realized and laboratory-scale demonstrations are limited to nominal power levels of several kW. Therefore, the TRL of SOE electrolysis systems can be estimated to be 5. The approximated specific investment of solid oxide electrolysis ranges from 1000-4000 €, as the technology has not passed the state of laboratory research [55]. Recent research has focused on reducing degradation [80, 81, 82].

5.1.3 Concentrated Solar Power (CSP)

Solar Towers, parabolic troughs, solar dishes and linear Fresnel are the four concentrated solar power technologies (see Figure 16), which can deliver electricity – and heat if required – to the electrolyzer system.

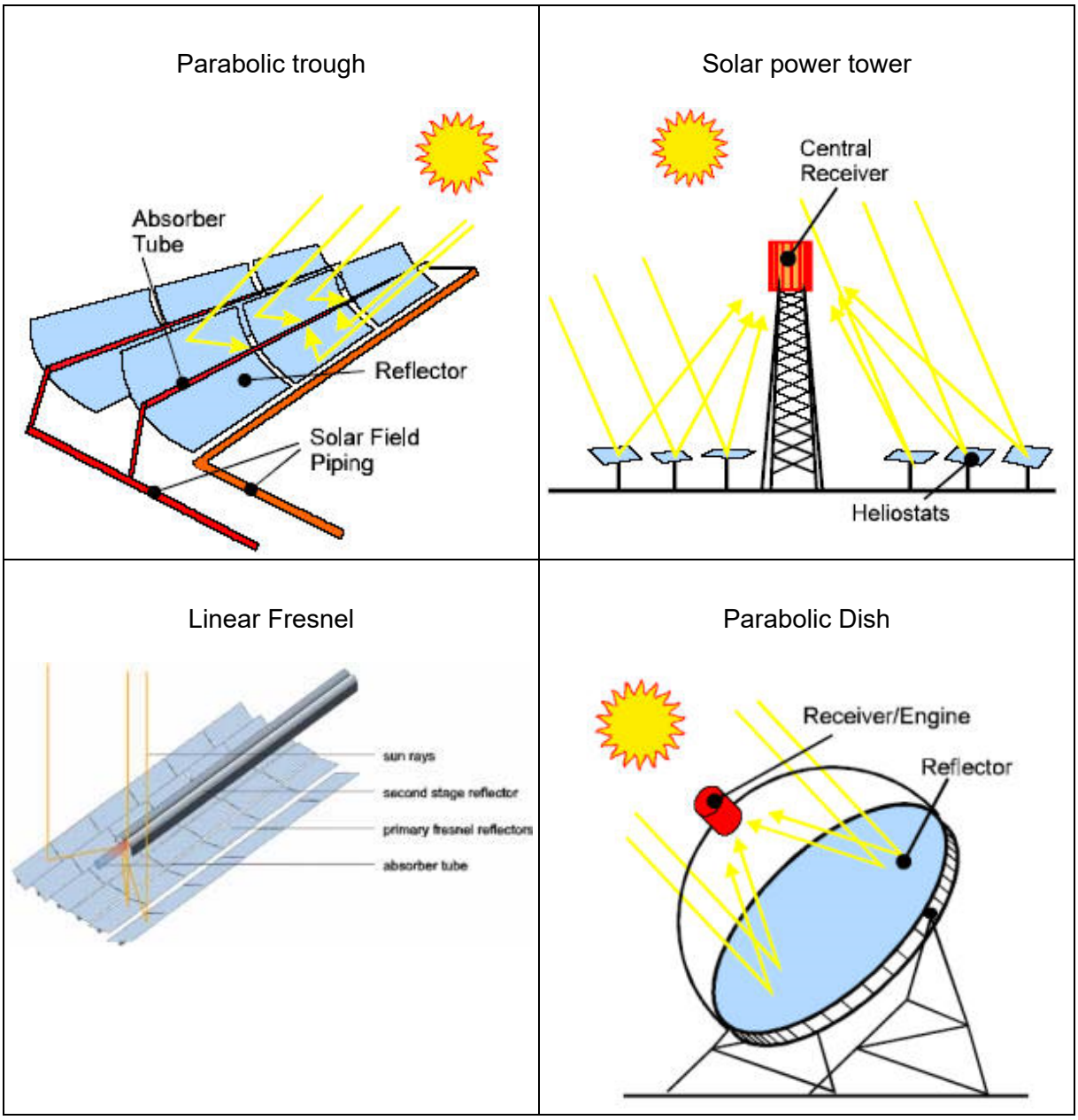

Figure 16. CSP technologies [83].

The solar tower technology is a large-scale system that utilizes many large, computer-controlled, sun-tracking mirrors, so-called heliostats, to focus sunlight on a receiver at the top of a tower. This receiver transforms the solar radiation into heat. A heat transfer fluid heated in the receiver then absorbs the highly concentrated radiation reflected by the heliostats and converts it into thermal energy. This heat is usually coupled to a conventional steam cycle through a heat exchanger to produce electricity. This technology enables operation at a high temperature level and provides heat storage capacities. Solar towers typically stand about 75-150 m height [84]. These plants are best suited for utility-scale applications in the 10-200 MW_e range [85]. This technology is commercially proven. The process design of the plant depends on the heat transfer fluid, which can be water, molten salt or air. In this study, the focus is on molten salt solar towers due to its superior energy storage capacity. In a molten salt solar tower, the heat transfer fluid used in the solar receiver to convert the collected solar

radiation into heat consists of molten salt which is typically a mixture, by-weight, of 60% sodium nitrate and 40% potassium nitrate. The molten salt is pumped from a large storage tank to the receiver at the top of the tower, where it is heated in tubes to a temperature of 565 °C. The hot salt is then returned to a second large storage tank where it remains until needed by the utility. At this point, the salt is pumped through a steam generator to produce the steam to power a conventional, high-efficiency steam turbine to produce electricity. Then, the cooled salt returns at a temperature of 285 °C to the first storage tank to be used in the cycle again. Due to the long-term molten salt thermal storage system that is normally integrated in these kinds of plants, it is possible to achieve 24 h operation during summer. Molten salts are indeed suitable for long-term storage due to their high thermal density and fluid properties at high temperature. The directly included storage system typically comprises a two-tank system: a “cold” one and a “hot” one. The molten salts from the “cold” tank feeds the solar receiver, are heated up and sent to the “hot” tank. As the steam generator is independently fed from the hot tank, the thermal storage system works as a buffer during solar transients and periods of no irradiance, so that the steam turbine’s operating conditions are stable. Thus, the first commercial molten salt power tower by Torresol Gemasolar can supply 15-hour full load equivalent heat storage capacity for a plant capacity of 12 MW_e [86]. As this plant is commercially-operated, it can be estimated that electricity generation by a molten salt solar power tower has achieved a high TRL of 9.

5.1.4 Photoelectrochemical (PEC) Water-Splitting

In photoelectrochemical solar-driven water-splitting, light harvesting and hydrogen generation are combined into a single monolithic device. In such devices, incident sunlight is converted into hydrogen using purely internally-biased electrolysis. Since at least one of the semiconductor surfaces is in contact with the electrolyte, the capital cost of a separate electrolyzer is avoided, potentially reducing the cost of the balance of plant, provided that chemically-stable materials are available.

One way to increase STH efficiency has been to use multi-junction semiconductors consisting of a photocathode and a photoanode to increase the utilization of incident photons, with an STH value of 8.2% reported [87]. Nevertheless, devices utilizing photoelectrodes are still at a low technology readiness level, as materials must still be found that best optimize the requirement for maximum utilization of the spectrum, a high open circuit voltage and long-term resistance to photoelectrochemical corrosion. Moreover, very few reports of solar-driven water-splitting devices based purely on photoelectrodes, of sizes approaching the m² range that would attract commercial interest, are available [88].

Yet, higher solar-to-hydrogen efficiencies approaching 10% have been achieved by using PV-PEC hybrid devices where the photovoltaic junction provides an additional bias, albeit at a higher material cost [89, 90]. Other options completely omit the use of photoelectrodes and instead monolithically-integrated, multijunction PV devices with electrocatalysts are used [91], achieving higher STH efficiency values of 10-22%. The highest STH efficiencies of devices measuring at least 50 cm² and using monolithically-integrated PV with electro-catalysts are,

however, still below 10% [92]. Despite the strides made in STH efficiency over the years, the device stability remains challenging and is the biggest barrier to large-scale deployment of PEC and related technologies for water-splitting. Therefore, we categorize these approaches as having a technology readiness level of 3 because the proof of concept has been shown but stability in both the laboratory and operational environment has not yet been validated.

5.2 Irradiation profiles of all locations considered in this study

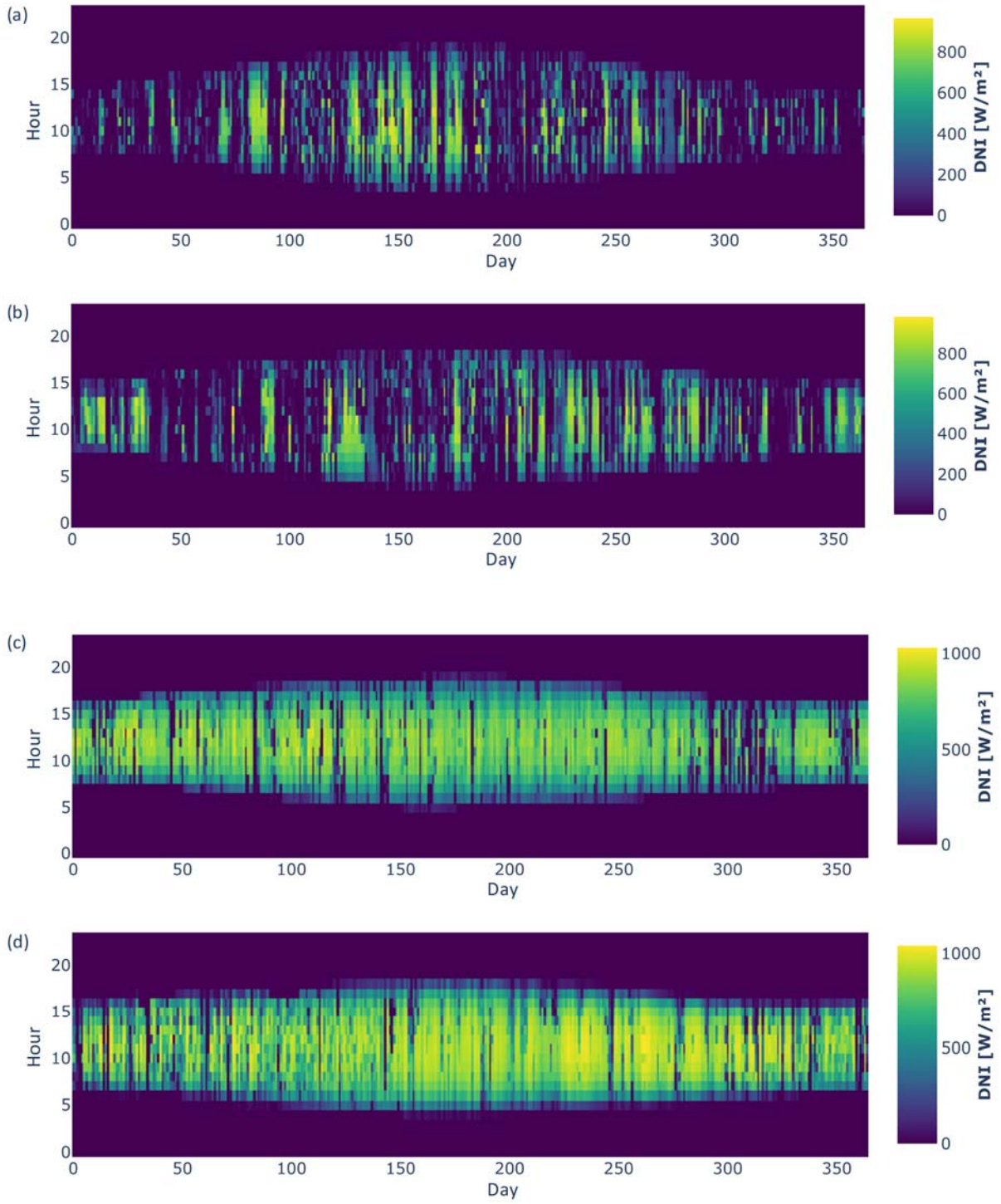

Figure 17. Irradiance profiles for Oldenburg/Germany (a), Freiburg/Germany (b), (c) Almeria/Spain (c) and Daggett/USA (d).

5.3 Hydrogen production quantities per location

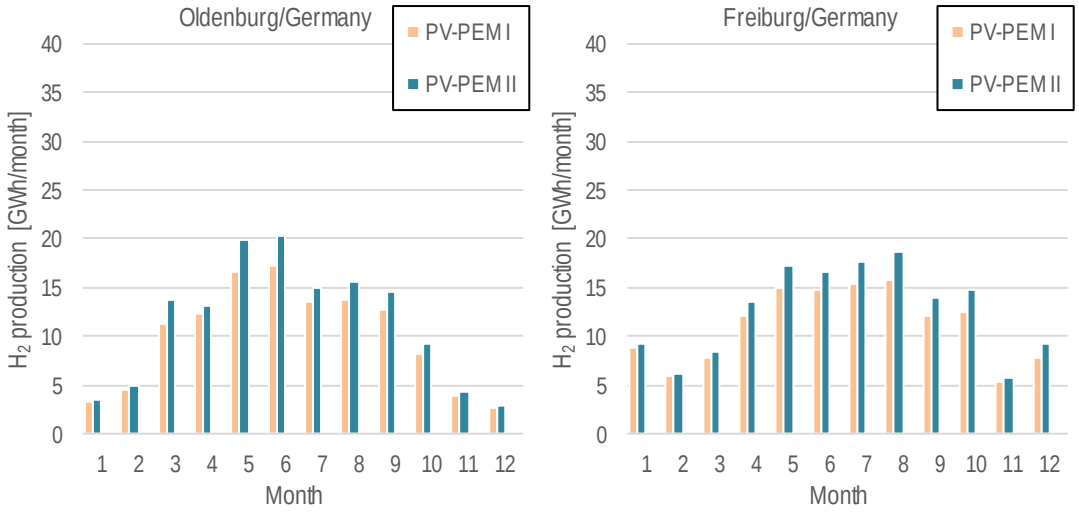

Figure 18. Annual hydrogen production quantities in Oldenburg and Freiburg in Germany (PV-PEM concepts only).

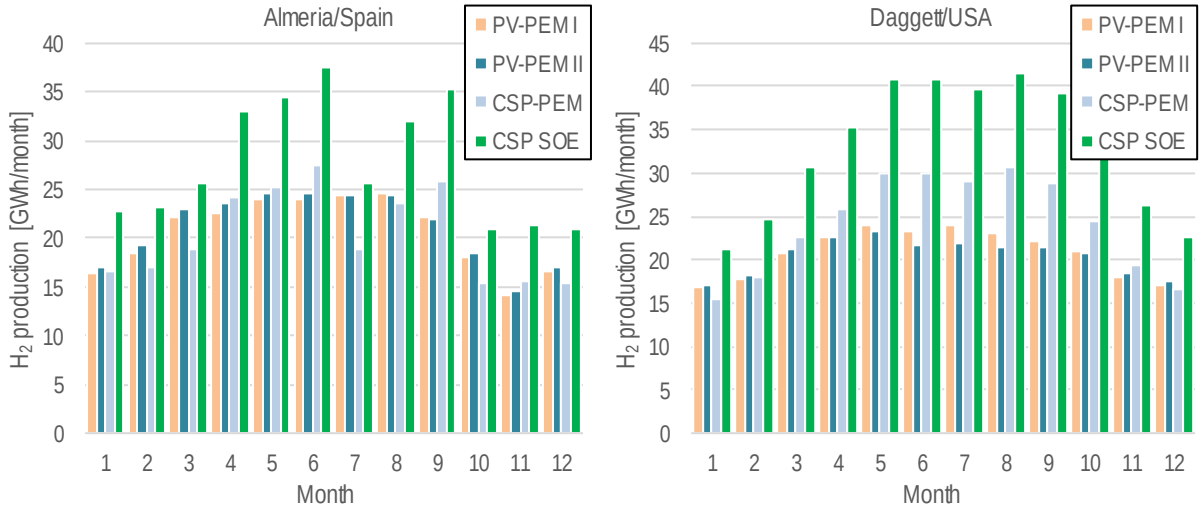

Figure 19. Annual hydrogen production quantities in Almeria/Spain and Daggett/USA (all concepts).

5.4 Sensitivity Analysis

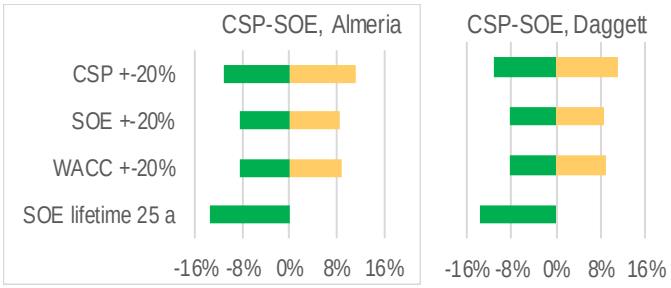

Figure 20. Cost sensitivities of the CSP-SOE for Almeria/Spain and Daggett/USA with unchanged conversion efficiency.

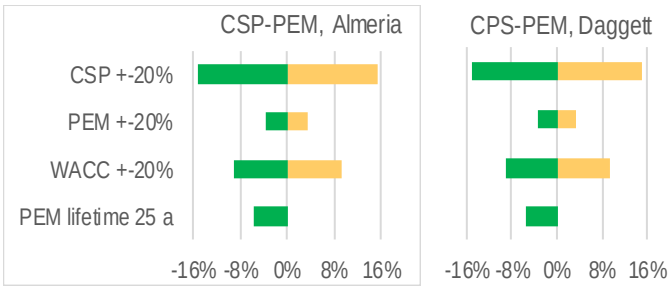

Figure 21. Cost sensitivities of the CSP-PEM for Almeria/Spain and Daggett/USA.

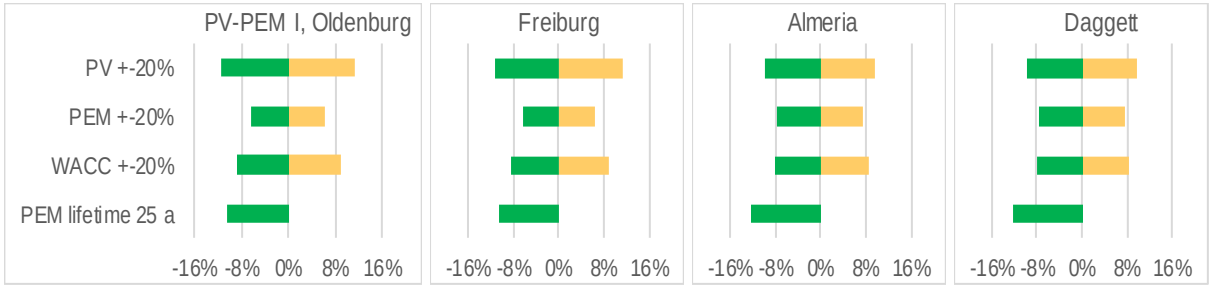

Figure 22. Cost sensitivities of the PV-PEM I for all locations.

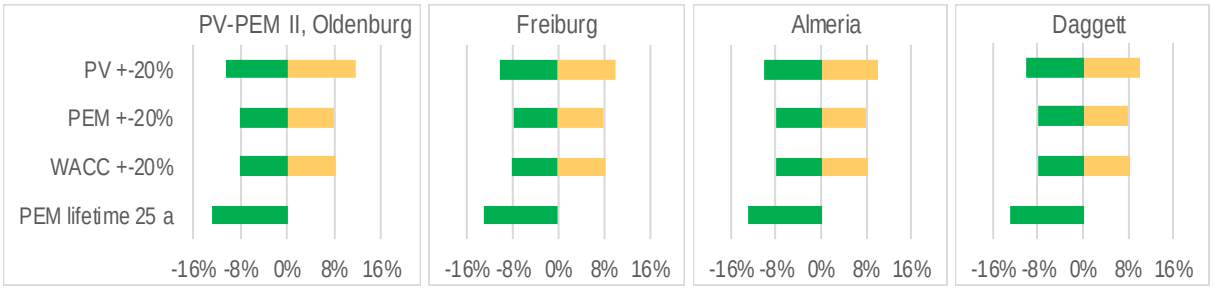

Figure 23. Cost sensitivities of the PV-PEM II for all locations.

5.5 Cost reduction potential

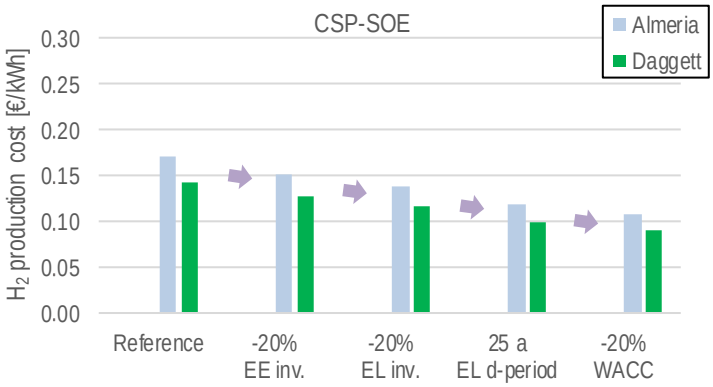

Figure 24. Cost reduction potential of the CSP-SOE concept with the energy conversion efficiency kept constant.

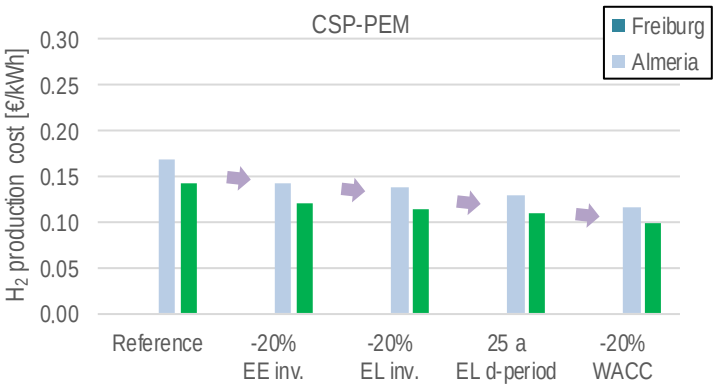

Figure 25. Cost reduction potential of the CSP-PEM concept with the energy conversion efficiency kept constant.

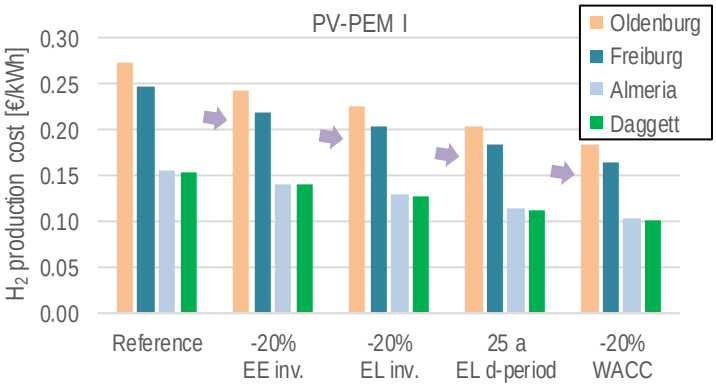

Figure 26. Cost reduction potential of the PV-PEM I concept with the energy conversion efficiency kept constant.

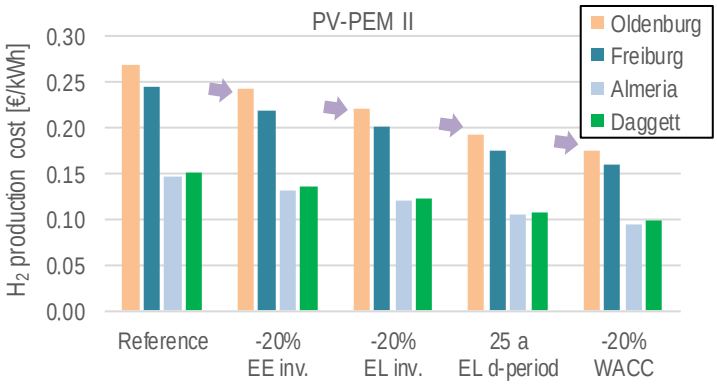

Figure 27. Cost reduction potential of the PV-PEM II concept with the energy conversion efficiency kept constant.